GAS DYNAMICS IN GALAXY CLUSTERS AND GALAXIES

DANIAL AHMAD BIN ARIFFIN LEE

FACULTY OF SCIENCE
UNIVERSITI MALAYA
KUALA LUMPUR

2020

GAS DYNAMICS IN GALAXY CLUSTERS AND GALAXIES

DANIAL AHMAD BIN ARIFFIN LEE

DISSERTATION SUBMITTED IN FULFILMENT OF THE REQUIREMENTS FOR THE DEGREE OF MASTERS OF SCIENCE

DEPARTMENT OF PHYSICS
FACULTY OF SCIENCE
UNIVERSITI MALAYA
KUALA LUMPUR

2020

UNIVERSITI MALAYA

ORIGINAL LITERARY WORK DECLARATION

Name of Candidate: **DANIAL AHMAD BIN ARIFFIN LEE**

Matric No: **SGR150049**

Name of Degree: **Masters of Science (MSc.) Physics**

Title of Project Paper/Research Report/Dissertation/Thesis ("this Work"): **GAS DYNAMICS IN GALAXY CLUSTERS AND GALAXIES**

Field of Study:

EXPERIMENTAL PHYSICS

I do solemnly and sincerely declare that:

(1) I am the sole author/writer of this Work;
(2) This Work is original;
(3) Any use of any work in which copyright exists was done by way of fair dealing and for permitted purposes and any excerpt or extract from, or reference to or reproduction of any copyright work has been disclosed expressly and sufficiently and the title of the Work and its authorship have been acknowledged in this Work;
(4) I do not have any actual knowledge nor do I ought reasonably to know that the making of this work constitutes an infringement of any copyright work;
(5) I hereby assign all and every rights in the copyright to this Work to the University of Malaya ("UM"), who henceforth shall be owner of the copyright in this Work and that any reproduction or use in any form or by any means whatsoever is prohibited without the written consent of UM having been first had and obtained;
(6) I am fully aware that if in the course of making this Work I have infringed any copyright whether intentionally or otherwise, I may be subject to legal action or any other action as may be determined by UM.

Candidate's Signature Date:

Subscribed and solemnly declared before,

Witness's Signature Date:

Name:

Designation:

GAS DYNAMICS IN GALAXY CLUSTERS AND GALAXIES

ABSTRACT

This thesis presents the results from a search for Neutral Hydrogen (HI) for the central region of the galaxy clusters A426 and A1367 using a 7m radio telescope. The resulting beam is substantially larger than previous studies, covering the central 2.5–3 Mpc diameter of these clusters. The detection of HI allows the mass of atomic gas associated with the cluster core to be estimated. The HI is not associated with any particular cluster member but present due to ram pressure and tidal stripping or recombination of intracluster gas. Overall results have revealed the presence of a significant mass of atomic hydrogen gas with relatively narrow velocity dispersion in the cores of A426 and A1367. The dynamics and evolution of clusters is highly dependent on the environment around the galaxies themselves. The parameters of these galaxies give an insight into how clusters function. Two spiral galaxies, NGC 1068 and NGC 1097, are used as case studies. Data from the Atacama Large Millimeter/Sub-millimeter Array (ALMA) and Mapping Nearby Galaxies at Apache Point Observatory (MaNGA) were used. The ALMA data uses Carbon Monoxide (CO) to uncover the rotation curves in the inner regions of the spiral galaxies. The rotational velocity of the galaxy proved useful in classifying them. The mass of HI in the A426 cluster was $(3.2 \pm 0.4) \times 10^{10}$ solar masses, with the A1367 has $(1.6 \pm 0.4) \times 10^{11}$ solar masses. For A426 and A1367 the detected HI gas is not consistent with the velocity range of the gas-rich spiral galaxies known within each cluster, leaving open the possibility that this cool atomic gas traces the gas cooling out of the intracluster medium in the cores of the cluster.

Keywords: Galaxy Clusters, Neutral Hydrogen, Gas

DINAMIK GAS DALAM GUGUSAN GALAKSI DAN GALAKSI

ABSTRAK

Tesis ini merangkumi keputusan dalam pencarian Hidrogen Neutral (HI) untuk kawasan pertengahan gugusan galaksi A426 dan A1367 dengan menggunakan teleskop radio 7m. Luas isyarat yang terhasil adalah lebih besar berbanding penyelidikan terdahulu, merangkumi 2.5-3 Mpc kawasan pertengahan gugusan. Pengesanan HI membolehkan jisim gas atomik yang berkait dengan teras gugusan dianggarkan. HI tersebut tidak berkait dengan mana-mana ahli gugusan, tetapi wujud kerana pelucutan tekanan "ram" dan tarikan graviti serta penggabungan semula gas. Secara keseluruhan, terdapat jumlah gas HI yang banyak dengan julat kelajuan yang kecil di kawasan teras A426 dan A1367. Dinamik dan perubahan sesuatu gugusan amat bergantung kepada keadaan persekitaran dalam gugusan tersebut. Galaksi dalam gugusan juga memberi gambaran terhadap cara gugusan berfungsi. Dua galaksi pilin, NGC 1068 dan NGC 1097, dipilih sebagai kajian kes. Data yang digunakan diperoleh dari Atacama Large Milimeter/Subilimeter Array (ALMA) dan Mapping Nearby Galaxies at Apache Point Observatory (MaNGA). Data Karbon Monoksida (CO) daripada ALMA digunakan untuk menghasilkan lengkungan putaran untuk bahagian pusat galaksi pilin. Kelajuan putaran galaksi membolehkan klasifikasi galaksi dilakukan. Jisim HI untuk A426 adalah sebanyak $(3.2 \pm 0.4) \times 10^{10}$ jisim suria, manakala dalam A1367 adalah sebanyak $(1.6 \pm 0.4) \times 10^{11}$ jisim suria. Dalam kes A426 dan A1367, gas HI yang dikesan tidak konsisten dengan julat kelajuan galaksi pilin yang kaya dengan gas. Hal ini membuka ruang kepada kemungkinan gas sejuk ini menunjukkan aliran keluar gas daripada kawasan teras gugusan.

Kata kunci: Gugusan Galaksi, Hidrgoen Neutral, Gas.

ACKNOWLEDGEMENTS

Many thanks go to Dr Christine Jordan, who helped us with the Jodrell Bank 7m Radio Telescope observations. Also not forgotten are Assoc. Prof. Dr. Zamri Zainal Abidin, who is my supervisor and Prof. Alastair Edge, who assisted me a lot. I am also very grateful to Mohd. Shaiful Rizal Hassan, Ungku Ferwani Salwa Ungku Ibrahim and other members of the Radio Cosmology Lab for their help and contribution. Special thanks are also given to Universiti Pendidikan Sultan Idris (UPSI), especially to Wan Zul Adli. Finally, I would like to thank both my parents for their moral support.

TABLE OF CONTENTS

LIST OF FIGURES

LIST OF TABLES

LIST OF SYMBOLS AND ABBREVIATIONS

A426	:	Abell 426 / Perseus Galaxy Cluster
A1367	:	Abell 1367 / Leo Galaxy Cluster
AGN	:	Active Galactic Nuclei
ALMA	:	Atacama Large Millimeter/submillimeter Array
CO	:	Carbon Monoxide
DR15	:	Data Release 15
GBT	:	Green Bank Telescope
HI	:	Neutral Hydrogen
ICM	:	Intracluster Medium
MaNGA	:	Mapping Nearby Galaxies at Apache Point Observatory
NGC	:	New General Catalog
NRAO	:	National Radio Astronomy Observatory
SDSS	:	Sloan Digital Sky Survey
UPSI	:	Universiti Pendidikan Sultan Idris

LIST OF APPENDICES

CHAPTER 1: INTRODUCTION

Research of astrophysical objects has progressed a lot in recent years. Observations and analysis of galaxy clusters and individual galaxies themselves has seen a marked increase in both quantity and quality. Some terminology and instruments need to be introduced as they essential to this research.

1.1 Dynamics of Galaxy Clusters

Before heading further, it is important to define what a galaxy cluster is. A cluster is called as such when 50 or more galaxies are placed together in a volume of space, making sure that they are gravitationally bound to each other (Abell,1958). Most galaxies in the universe are found being bundled together.

The name Abell comes from George Odgen Abell, who first did the survey on galaxy clusters in the sky as his PhD research (Abell,1958). This list is known as the Abell catalog. Two of the clusters, Abell 426 and Abell 1367 were used here. The reasons for choosing them will be covered in Section 3.1.

1.1.1 Neutral Hydrogen

Hydrogen is the most abundant element in the universe. Current models seem to suggest that most of the hydrogen in the universe. Hydrogen exist in three flavors, Molecular Hydrogen (H_2), Neutral Hydrogen (HI) and Ionized Hydrogen (HII). Of the three, HI is probably the useful for radio astronomy in general as it is the source of the 21cm radiation. This radiation comes from the spin-flip transition of the hydrogen atom.

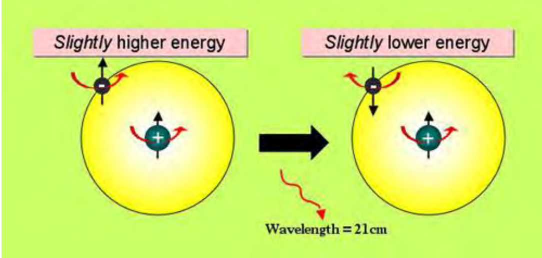

Figure 1.1: Spin-Flip transition in Hydrogen (Picture Credit: Swinburne Astronomy Online)

The spin-flip transition is the side-effect of the hyperfine splitting of the hydrogen atom. Electrons have a property known as spin. In the hydrogen atom, if the proton and electron have parallel spins, the energy contained is slightly higher when compared to the anti-parallel position.

In nature, things tend to want to stay or decay to the lowest possible energy state if left alone. Similarly, the hydrogen atom in our case wants to in the most relaxed state allowed. To achieve this, the electron changes the direction of its spin. In doing so, a single photon with the wavelength of 21cm was released. Note that the probability of a single atom undergoing this transition is extremely remote.

However, the number of hydrogen atoms in the universe is very large. This increases the probability of this transition happening. The 21cm emission is unique to neutral hydrogen. In terms of frequency, this translates to about 1.42GHz.

1.1.2 Carbon Monoxide (CO)

After HI, the next molecule of importance in astrophysics is Carbon Monoxide (CO). CO has a variety of subspecies, with the most abundant being ^{12}CO. This is since the most abundant isotope of carbon is Carbon-12. Other possible species of CO include ^{13}CO, $C^{17}O$ and $C^{18}O$. Each of them has its own emission frequency that allows it to be detected. This emission also differs according to the transition of the quantum energy state of the molecules. For example, ^{12}CO with a Quantum Number transition of 1-0 has a rest-frame emission of 115.27GHz. The same molecule has an emission at 345.80 GHz if a 3-2 transition takes place.

CO is very useful when studying galaxies, especially in their central regions. The asymmetric nature of CO (The oxygen atom is bigger than the carbon atom) allows it more degrees of freedom which contributes to the emission detected. In contrast, H_2 being a symmetrical molecule, does not have this much degree of freedom. Hence, especially in radio wavelengths, H_2 is almost impossible to detect even though its abundance is very high especially in star forming regions. In its place, CO is used as a tracer of H_2. CO has the added advantage that its molecules are resistant towards dissociation.

1.1.3 Hydrogen Alpha

Unlike HI and CO, Hydrogen Alpha (H-Alpha) emission occurs in the optical wavelength. H-alpha emission comes from the dropping of the electron in a hydrogen atom from a higher excited state to the second excited state. For the field of extragalactic science, H-Alpha tends to be used to study star formation in galaxies. It could also be used to study the kinematics of the galaxies.

1.1.4 Other Molecules

Besides the atoms and molecule mentioned above, there are other important molecules in astrophysics. For example, HCN, HCO, Methanol and Formaldehyde are very useful for probing star forming regions in galaxies. This is due to the high relative concentrations of these molecules in molecular clouds and nebulae. Some molecules are also easily dissociated when the surrounding temperature increases such as when nuclear fusion starts, and a star is born.

1.2 Radio Telescope Basics

A basic radio telescope system can be divided into two parts; a front end and a back end. The job of the front end is basically just to collect the incoming signals from a source. The parabolic dish concentrates the signal. The signal is also pre-amplified before being passed to the back end.

At the back end, the signal is further amplified until it is strong enough to be analysed. Band pass filters are used to filter out unwanted frequencies. The collected data is then stored or passed to another computer to be analysed. Other parts of the back end include the systems control, which functions to position the telescope in the appropriate direction, directs observations, and monitors the receiving systems.

1.3 The Jodrell Bank 7m Radio Telescope

The most promising route to search for any, more diffuse HI gas is to use a radio telescope with a large beam (and hence small diameter) and observe relatively local galaxies.

The galaxy cluster observations were conducted using the Jodrell Bank 7m Telescope. This telescope originally started life as at a rocket testing facility in Woomera, Australia. When the front end (the reflector dish) was transferred to Jodrell Bank, it was fitted with new drive systems and receivers. Currently, it is mainly used by the undergraduates of the University of Manchester.

The telescope is equipped with a 21cm receiver and 5 MHz, or 1050 km s^{-1}, bandwidth sampled by a 64-channel filter-bank. The width of a channel is 10 kHz, or 2.1 kms^{-1}, and was used to observe the 21cm line corresponding to the frequency of 1420 MHz. The main beam of the telescope is about 138 arcmin. The available tuning range of 1365 MHz to 1435 MHz allowed HI to be studied within a redshift of 0. 040.This puts it in a very useful position to observe the galaxy clusters used in this research.

Figure 1.2: The Jodrell Bank 7m Radio Telescope on the right. The radio telescope in the background is the 64m Lovell Telescope. (Picture Credit: Mike Peel; Jodrell Bank Centre for Astrophysics, University of Manchester)

1.4 The UPSI-UM Radio Telescope

Radio telescope is located at the Universiti Pendidikan Sultan Idris (UPSI) campus at Tanjung Malim, Perak. Figure 1.3 shows the radio telescope. The specifications for this telescope are listed in Table1.1. The L-band receiver that is to be installed at this telescope has been tested at the Korea Astronomy and Space Science Institute (KASI). At the time of writing of this thesis, the pointing accuracy of the telescope is being upgraded. Since the specifications and capability of this telescope is quite like the Jodrell Bank telescope, it is intended that the science and knowledge that was gained from the 7m telescope be applied to this one.

Figure 1.3 The UPSI-UM radio telescope.

This work also investigated the feasibility of using the techniques learnt from the Jodrell Bank telescope on UPSI-UM telescope. Due to the limitation of the range of the azimuthal motion that can be covered by the UPSI-UM radio telescope, it is vitally important that the time of the object of interest is within the field of view of the telescope.

Table 1.1: Specifications of the UPSI-UM Radio Telescope.

Diameter	7.3m
Operating Frequency	1.1-1.5 GHz
Antenna Type	Dual Refelector
Antenna Noise Temperature	43K
Beamwidth	2.05 Degrees

1.5 The Atacama Large Milimeter/submilimeter Array (ALMA)

The Atacama Large Milimeter/submilimeter Array (ALMA) is an interferometer located in the Atacama Desert of Chile. A total of 66 antennas (a mix of 7m and 12m diameter) forms the array. Its location was chosen specifically as it is the driest place known on Earth. Its elevation (5000m above sea level) was another reason for placing it here. The receivers of ALMA are tuned to a range of frequencies divided into bands. Currently, 8 out of the 10 bands are operational. The list of Bands is in Table 1.2.

Table 1.2: List of Observing Bands of ALMA.

Bands	Frequency Coverage (GHz)	Notes
1	35 - 50	Not Operational
2	60 - 90	Not Operational
3	84 - 116	Operational
4	125 - 163	Operational
5	163 - 211	Operational
6	211 - 275	Operational
7	275 - 373	Operational
8	385 - 500	Operational
9	602 - 700	Operational
10	787 - 950	Operational

For this thesis, only Band 7 was used. Band 7 of ALMA covers the emission frequency of Carbon Monoxide (CO) Quantum level 3-2 transition. This is particularly useful as CO is a very good tracer especially in the central regions of galaxies.

1.6 Mapping Nearby Galaxies at Apache Point Observatory (MaNGA)

The Mapping Nearby Galaxies at Apache Point Observatory (MaNGA) is a part of the Sloan Digital Sky Survey (SDSS). The telescope used is the 2.5m Sloan Foundation Telescope, located at Apache Point Observatory, New Mexico, USA. MaNGA operates at 360 – 10000 nm wavelength. MaNGA observes the entirety of galaxies (about 10000 nearby galaxies with redshifts less than 0.03) across its optical fibres.

The data used comes from Data Release 15 (DR15). DR15 is the third data release in the 4th phase of the SDSS. The observations took place mainly in July 2017. SDSS data releases are cumulative however, so earlier data releases are included in DR15.

1.7 Summary

This thesis can be broadly divided into two parts, namely observations on galaxy clusters and observations of individual galaxies.

This research is intended to meet the following:

a) Objectives:

1. To measure the mass of HI in two galaxy clusters, namely the Perseus Cluster (Abell 426) and the Leo Cluster (A1367).
2. To plot the rotation curve of the galaxies NGC 1068 and NGC 1097 using CO as the tracer and identify any defining characteristics of Compton-thick AGN.
3. To investigate the gas dynamics of spiral galaxies using H-alpha emission and HI using MaNGA public data.

b) Problem Statement:

The study of gas dynamics in galaxies within the environment of galaxy clusters is lacking in previous literature especially with regards to HI as previous observations mostly require the use of large radio telescopes.

c) Novelty:

1. Observations of galaxy clusters as a whole with a small radio telescope has hardly, if ever, been done.
2. Comparisons of the central regions of Compton-thick AGNs with non-Compton-thick AGNs in radio frequency have not been attempted.
3. The gas dynamics of H-alpha in galaxies being compared directly with the HI present.

CHAPTER 2: LITERATURE REVIEW

Observations of galaxies and galaxy clusters have been done for quite some time. However, radio observations in particular only started in the 20th century with the Neutral Hydrogen (HI) in the Milky Way.

2.1 Galaxy Clusters

2.1.1 Observations and Science with a Small Radio Telescope.

The commonness and detectability of HI makes it a very powerful tracer of gas in many different areas in the Universe. Despite being the most abundant element, one environment in which it appears to be lacking is the cores of clusters of galaxies. As an example, Solanes et al. (2001) found that there are indications of HI deficiency within the spirals of many galaxy clusters. The depletion levels became especially significant for galaxies that are close to or in the central regions of galaxy clusters.

Therefore, we cannot reject the possibility that the HI being detected is located in the space between the galaxies. Over the years, various theories have been put forward to explain the lack of HI. One of the first was by Gunn & Gott (1972), who came up with ram-pressure stripping.

A galaxy may pass through the cluster core on its orbit around the cluster. As it moves toward the cluster centre, the hot intracluster gas starts to strip the HI in the outer parts of the galaxy. This is analogous to the Earth's atmosphere stripping material of a meteoroid on its journey to the surface. The deeper the galaxy gets in the central regions, the more intense this process is. In extreme cases, it is possible for the galaxy to be stripped clean of HI. Examples of extreme ram-pressure stripping are observed at low redshift in systems like ESO137001 in A3627 (Fossati et al. 2016) where a HI tail is found with the discovery of `Jellyfish' galaxies (Ebeling et al. 2014) where the stars formed from the stripped gas are most prominent. The cold gas content of galaxies can also be depleted by being converted into stars. Research on the Fornax cluster by Schroeder et al. (2001), shows there is an excess of star formation in the galaxies where the HI detections were made. Other mechanisms that contribute towards HI depletion are thermal conduction and viscous stripping.

One final potential source of HI gas is from the cooling of the hot, diffuse intracluster medium that is present in the cores of most clusters (Fabian,1994). The detection of cold molecular gas in the cores of clusters in which the cooling is strongest Edge (2001) and Salome & Combes (2003) suggests that a significant mass of cooled gas is present. Recent results from Hitomi (Aharonian et al. 2016) demonstrate that the intracluster gas does not share the dynamics of the member galaxies and is relatively quiescent dynamically with velocity widths comparable to those seen in the cold molecular gas and not the velocity dispersion of the member galaxies. Therefore, it may be possible to use HI as an additional tracer of cooled gas in cluster cores.

For this thesis, two local, X-ray bright clusters were selected, namely the Perseus cluster (A426) and the Leo cluster (A1367). A426 is the brightest cluster of galaxies in the X-ray band and has been studied extensively over the past 40 years (Fabian et al. 2000). The central galaxy of this cluster, NGC1275, is a strong radio source, 3C84, and known to vary significantly Dutson et al. (2014). A1367 is the next X-ray brightest cluster with strong cooling in the northern hemisphere (Edge et al. 1990) within a redshift of 0.03 so a very suitable target to compare to A426. A1367 also has a strong radio source, 3C264, in its brightest central galaxy, NGC3862.

Before going further, the alternate names of the two clusters need to be addressed. The International Astronomical Union (IAU) has divided the sky into 88 regions, each named after a constellation. The name Perseus comes from the location of the galaxy cluster in the sky, which is in the constellation Perseus. Similarly, the Leo cluster was named for its location in the constellation Leo.

Optical observations of A426 includes the work of Brunzendorf & Meusinger (1999) which was done using the Tautenberg telescope in 1999, listing 660 galaxies in their catalogue covering the full extent of the cluster. In addition, more targeted HST observations of the central regions of A426 have made several discoveries. In Penny et al. (2009) they discovered that the out of the 25 dwarfs in the sample, 12 of them require dark matter to hold them together in the cluster potential. The next part was done by De Rijcke et al. (2012) who looked at the global photometric scaling relations in elliptical or early-type galaxies. They found that these galaxies obey a single colour-magnitude relation, which they stated to be a luminosity-metallicity relation for old stellar populations. Part three of this research (Penny et al. 2011), they studied the way the environment in the Perseus cluster affects the characteristics of the dwarf galaxies there. The parameters used were concentration, asymmetry and clumpiness in order to sort the morphologies of the dwarfs. This time, they looked at the outer parts of the Perseus cluster and identified 11 dwarf elliptical and dwarf spheroidal galaxies which have not been detected previously. When compared to other dwarf galaxies that are located in the more central regions of the Perseus cluster, the dwarfs in the outskirts of the cluster are more disturbed than the ones in the core. Lastly, Penny et al. (2012) searched for Ultra Compact Dwarfs (UCDs) around the central galaxy of Perseus NGC 1275. At a distance of 250 kpc from the cluster centre, they found indications that proto-globular clusters and proto UCDs are currently forming in the cluster. The morphology of these dwarf galaxies is much smoother in the central 300 kpc of the cluster than equivalent galaxies at larger radii suggesting a much lower gas content (and hence much less recent star formation) in systems in the cluster core.

The Leo galaxy cluster (Abell 1367), is currently undergoing a merger. The evidence to support this comes from Donnelly et al. (1998), who used X-ray emissions to map the temperature of central regions of the cluster. Their results suggest the beginning stages of merging between two sub-clusters along a southeast-northwest axis. Further dynamical analysis of this comes from Cortese et al. (2004). Their work utilised 146 member galaxies to derive a non-Gaussian velocity distribution. They also pointed out the existence of star-forming galaxies that are currently infalling towards the core of the South-east sub cloud. A multiple merger scenario was proposed by Sun & Murray (2002) as well as Churazov et al. (2003), with results from the Chandra and XMM-Newton results respectively. The evidence points to cool gas currently streaming into the cluster core. HI observations of A1367 has mostly focused on the individual galaxies themselves. More recent work by Ge et al. (2019) reveals a merger shock in the north-western edge of the cluster. They postulated that the two sub-clusters passed through each other approximately 700 million years ago. This was based on the position of the Brightest Cluster Galaxies (BCGs) of the cluster, namely NGC 3842 and NGC 3682.

The method used, i.e. using a small radio telescope to observe the HI in a galaxy cluster in one go instead of observing the galaxies of the cluster one at a time, has been done by Hassan et al. (2016) by observing the cluster Abell 262.

Table 2.1: Parameters of the Perseus Cluster

Name of Cluster	Abell 426 @ Perseus Cluster
Redshift	0.0179
Size	863.0 arc minutes
Number of Galaxies	660 Galaxies
Celestial Coordinates (Epoch J2000)	Right Ascension: 03h 19m 47.2s Declination: +41° 30’47”

Table 2.2: Parameters of the Leo Cluster

Name of Cluster	Abell 1367 @ Leo Cluster
Redshift	0.0220
Size	266.0 arc minutes
Number of Galaxies	363 Galaxies
Celestial Coordinates (Epoch J2000)	Right Ascension: 11h 42m 1.0s Declination: $+19^{o}$ 45’32”

2.1.2 Observations of Galaxy Clusters with other Telescopes.

Lah et al. (2009) utilized the Giant Metrewave Radio Telescope (GMRT) in Pune, India to observe the galaxy cluster Abell 370. A total of 324 galaxies were observed which yielded a HI mass of 6.6 x 10^9 solar masses. If only the ‘blue’ galaxies (galaxies with substantial star formation activities) were considered, the HI mass reduces to 19.0 x 10^9 solar masses.

2.2 Observation of Individual Galaxies

The spiral galaxy NGC 1068 was one of the nearest of the ‘Active galaxies’ to Earth. An active galaxy, or more accurately an Active Galactic Nuclei (AGN), is a galaxy (be it spiral or elliptical) whose central region or nucleus is brighter than just the light form all the stars combined. The engine that causes this brightness is a supermassive black hole. NGC here stands for New General Catalogue, a listing of nebulae and galaxies.

NGC 1068 is an example of a Seyfert Galaxy. Seyferts are named after Carl Seyfert, who in 1943 identified certain spiral galaxies with unusually bright centers. Seyferts can be divided into two types; Type 1 Seyferts and Type 2 Seyferts. Simply put, Type 1 Seyferts are defined by the position of the two emission lines, while Type 2 Seyferts have only the narrow emission line. NGC 1068 is an example of a Type 2 Seyfert. The basic parameters of this galaxy are shown in Table 2.3.

The galaxy NGC 1097 is another Seyfert galaxy. In this case, it is a Type 1 Seyfert galaxy. The parameters of this galaxy are shown in Table 2.4

Table 2.3: Parameters of the Galaxy NGC 1068.

Parameters	Value
Right Ascension	2h 42m 40.7s
Declination	-0d 0m 48s
Inclination Angle	40 degrees
Redshift	0.003793
Morphological Type	SAb C

Table 2.4: Parameters of the Galaxy NGC 1097.

Parameters	Value
Right Ascension	2h 46m 19.0s
Declination	-30d 16m 19.0s
Inclination Angle	41.7 degrees
Redshift	0.00424
Morphological Type	SAb C

Before progressing further, it should be noted that there is a further level of classification for AGNs. NGC 1068 is an example of a Compton-thick AGN. A Compton-thick AGN occurs when the density of material in the torus, namely the HI column density, N_H, is higher than the inverse Thomson cross-section of 1.5 x $10^{-24}cm^{-2}$. NGC 1097 is not a Compton-thick AGN.

Being close to Earth, NGC 1068 has been extensively studied especially in the X-ray wavelengths. Among the previous research that has covered this particular area is the work by Marinucci et al. (2016). Here, the authors have stated that based on the Nu-STAR and XMM-Newton data, no spectral variation below 10keV was found. Tsai et al. (2012) has done CO observations of NGC 1068. Their work used the CO(3-2) data from the Submilimeter Array and Owens Valley Radio Observatory Millimeter Array. Impellizzeri et al. (2019) has also observed NGC 1068 and found that there are two nested counter rotating disks in the center.

For the case of NGC 1097, Onishi et al. (2015) also used ALMA data to derive the mass of the supermassive black hole in NGC 1097 using HCN and HCO molecules. They deduced that the black hole has a mass of 1.4 x 10^8 solar masses. Earlier, Izumi et al. (2013) conducted observations of the dense gas in NGC 1097 also using the ALMA data. Because of its orientation being almost face-on towards Earth, NGC 1097 has also been the target of star formation studies. In Tabatabaei et al. (2018), the authors found that there is a massive quenching of star formation in the center of NGC 1097. They compared the ratio of the mass of molecular clouds to the magnetic flux. Their findings indicate most of the molecular clouds are supported against gravitational collapse. This is important as star formation can only take place if the gas comes together. Prieto et al. (2019) studied NGC 1097 in wavelengths from Infrared to Ultraviolet. They resolved 247-star clusters in NGC 1097, with the cluster properties fitting with other known clusters in the Milky Way and other field galaxies.

We wish to investigate the rotation curve via radio wavelength observations in the central parts of Seyfert galaxies in order to carry out preliminary work to see is there any difference between Compton-thick and non-Compton thick AGNs in this region. This was done as studies of Compton-thick AGNs previously have mainly utilized X-ray, optical and infrared wavelengths. This was also partially inspired by the fact that the Brightest Cluster Galaxy (BCG) of Perseus cluster, NGC 1275 is also classified as a Seyfert, although morphologically, it is classified as a Peculiar galaxy. The rotation curve of galaxies has historically been the main driving point behind the introduction of dark matter into mainstream astrophysics.

The MaNGA data used in this thesis is intended to complement the HI observations of the clusters in Section 2.1. This is because in DR15, there is an additional component was added to the data set which was the HI observations of the galaxies in the MaNGA catalog. An example of this is the work of Masters et al. (2019), who carried HI follow-up for the MaNGA survey. They presented the results of observing HI of 331 galaxies within the MaNGA catalog using the Robert C. Byrd Green Bank Telescope. 181 galaxies show positive detection of HI. Related work is the effort of Lin et al. (2017), who studied the quenching of star formation and molecular gas in three green valley galaxies. The three galaxies are part of the MaNGA survey. Other works utilizing the MaNGA data such as Jin et al. (2019) used 149 early-type galaxies to look into their mass distributions and internal structures.

CHAPTER 3: METHODOLOGY

For clarity, this section has been split into three parts. However, it should be noted that all three parts were carried out roughly simultaneously.

3.1 HI Galaxy Cluster Observations

The heart of this research uses HI data obtained from a radio telescope. The first step in achieving this is cluster candidate selection. The starting point was the original Abell all sky catalog of 4073 galaxy clusters (Abell et al. 1989). The full list was then trimmed to around 1000 clusters by only selecting those clusters with an Abell richness of 2 and above. Further filtering was done by looking at the uniqueness of the clusters especially with regards to HI Observations. It was at this stage that A426 revealed itself. Previous literature has shown that the cluster has sound waves propagating in the cluster (Fabian et al. 2017). Hitomi (Aharonian et al. 2016) also found signs that the ICM in A426 is quiescent. These observations make it a good candidate to investigate the gas dynamics of a galaxy cluster. Previous HI observations have mainly targeted individual galaxies in clusters, such as De Young et al. (1973) who observed the central galaxy of A426, NGC 1275. In order to better probe the gas dynamics of the cluster, a new technique was devised in which a radio telescope with a size of around 7m was to be used to observe the cluster. This enables the entire cluster to be observed in one go instead of observing the individual galaxies of the cluster piecemeal. This would mean that if any Hi gas exists in the space between galaxies would be picked up as well. HI was chosen as the tracer as it is the most abundant element. It was this criteria that let to the choice of using he Jodrell Bank 7m Telescope.

A little history of the Jodrell Bank 7m Radio telescope. This telescope is located at the Jodrell Bank Centre for Astrophysics. Originally, the parabola was first built for tracking rockets in the 1970's in Woomera, Australia. It was then repurposed as a radio telescope by replacing the electronics such as 16-bit absolute encoders and proprietary drive systems for the azimuth and elevation controls.

The choice made in pairing the instrument and cluster allows the central region of the cluster, which fits our aim to study the gas dynamics there. However, as the field of view of the telescope on covers about 22% of A426, we also chose another galaxy cluster A1367 to be observed. This was intended to complement the results from A426. Observation of A1367 covers about 50% of the cluster. Long term, the HI observations carried out here is aimed at laying the ground work towards deeper exploration such as dark matter research.

Further support of this work was found in a paper by Battye et al. (2004). Within the aforementioned paper, the authors illustrated the relation of the beam size necessary to detect clusters at various high redshift values. We have extended the plot towards the lower redshift range where the two galaxy clusters are located in order to determine the minimum primary beam size (field of view) necessary to carry out observations. This is shown in Figure 3.1.

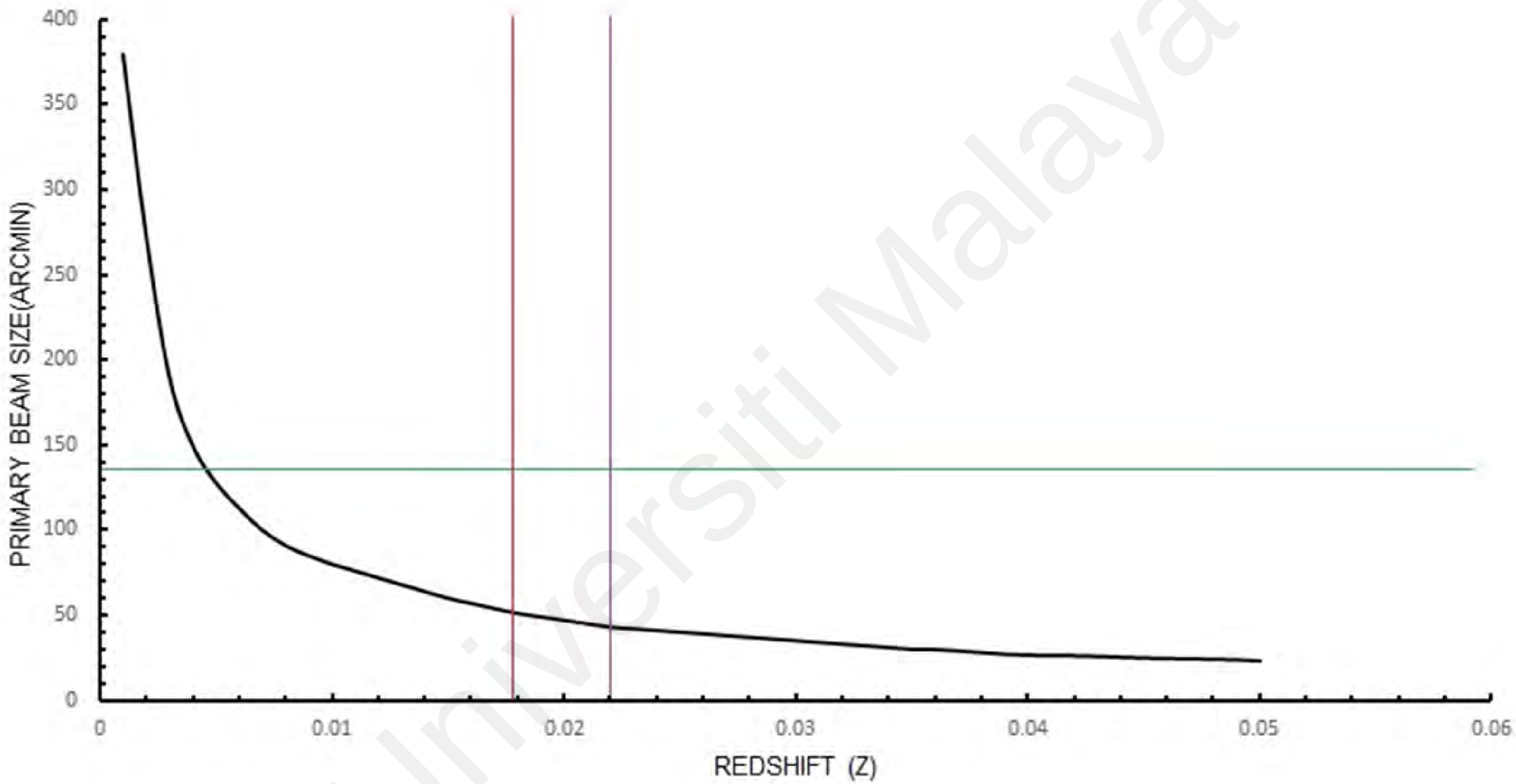

Figure 3.1: The graph showing the relation between the redshift of the object of interest and the minimum primary beam size necessary to detect such objects. The horizontal green line is the primary beam size of the Jodrell Bank 7m Telescope. The vertical red line marks the redshift of the A426 cluster at z=0.0178, while the vertical purple line indicates the redshift for the A1367 cluster.

The observation of A426 is well within the capabilities of the telescope. The specification of the 6.4 m radio telescope, with collecting area and pointing accuracy of about 38.22 m^2 and 0.03 arcmin respectively, allowed us to assess the HI contribution for A426 as a whole. This is opposed to observing just the individual galaxies in a particular cluster which requires a bigger telescope with higher sensitivity. Due to Doppler shift, the 1420 MHz HI signal from A426 is shifted to 1395 MHz. Observations of A426 were carried out along a 9-month period from October 2013 to July 2014. The total observation was 661 scans. Of this, 165 scans were usable, which translates to 165 hours of total observation time. The rest were rejected because of the high Radio Frequency Interference (RFI) levels especially during the May 2014 observing session. An example of the raw data is shown in Figure 3.2.

The same telescope at Jodrell Bank was also used to observe the galaxy cluster A1367. The observations took place over the same 9-month period as for the case of A426. The observations produced 579 scans. 138 scans were usable, which gives 138 hours' worth of observation time.

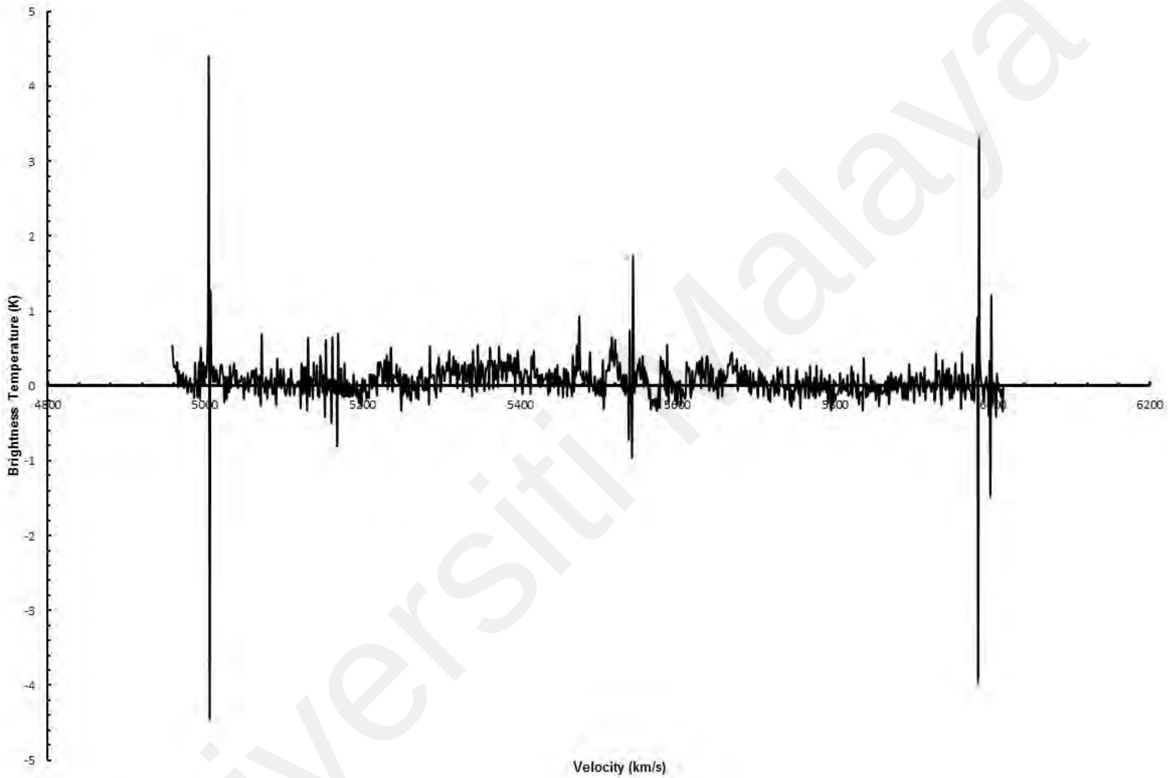

Figure 3.2 An example of the raw data spectra obtained from the telescope. In this case, this is for A426. Note the sharp spikes of Radio Frequency Interference (RFI).

3.2 CO Observation Data

The candidates chosen for this section were NGC 1068 and NGC 1097. NGC 1068 was chosen as it had been mapped before in HI such as by Brinks et al. (1998) who used the Very Large Array. Gallimore et al. (2003) investigated the HI absorption in NGC 1068. Similarly, NGC 1097 was chosen precisely because of previous HI observations such as Ondrechen et al. (1989) with the Very Large Array. To investigate the central regions of the galaxies, CO was used as its shorter wavelength and higher frequency than HI promises better resolution at the scales discussed here. Further reasons on the choice of NGC 1068 and NGC 1097 are found in Section 2.2. In contrast to Section 3.1, available public data were used for the part on individual galaxy observations. For the CO observations, ALMA data were used.

The data set used for NGC 1068 was Project 2011.0.00061S (Principle Investigator Takano, S). This observation used Band 7 of ALMA on the 9th and 10th of January 2012.Total integration time is 3024s with a velocity resolution of 0.85 kms^{-1}. The 16 antennas used was in the compact configuration. The flux calibrator used was Callisto, one of the moons of Jupiter.

For NGC 1097, the data came from project 2011.0.00108.S (Principle Investigator Kohno,K). This observation also used the Band 7 of ALMA. Total integration time was 2903.04 seconds with a velocity resolution of 0.82 kms^{-1}. The flux calibrator used was the planet Mars. For both of these projects, the molecule observed was CO (3-2).

3.3 MaNGA Data

The MaNGA data was obtained from the Sloan Digital Sky Survey Data Release 15 (SDSS DR15). The data is publicly available at the SDSS server and can be downloaded by anyone. For DR15, the analysis of the data was done with the newly introduced software called MARVIN. The HI data comes from the HI-MaNGA Data Release 1, being one of the Value Added Catalogs in MaNGA. To date, they have been allocated 192.5 hours of observation time in 2016 at the the Robert C. Byrd Green Bank Telescope (GBT) which is located in West Virgina, United States. The next year, 1097 hours were allocated.

A sample of 10 galaxies were chosen with the caveat that the galaxy has been observed both in MaNGA and by the GBT. The released HI data carries the ID AGBT16A_095. The sample script for downloading the data is included in Appendix A. This sample consists of spiral galaxies with varying orientations (Some are face-on while others are almost edge-on). Hydrogen Alpha has been chosen to make the comparison with HI more valid.

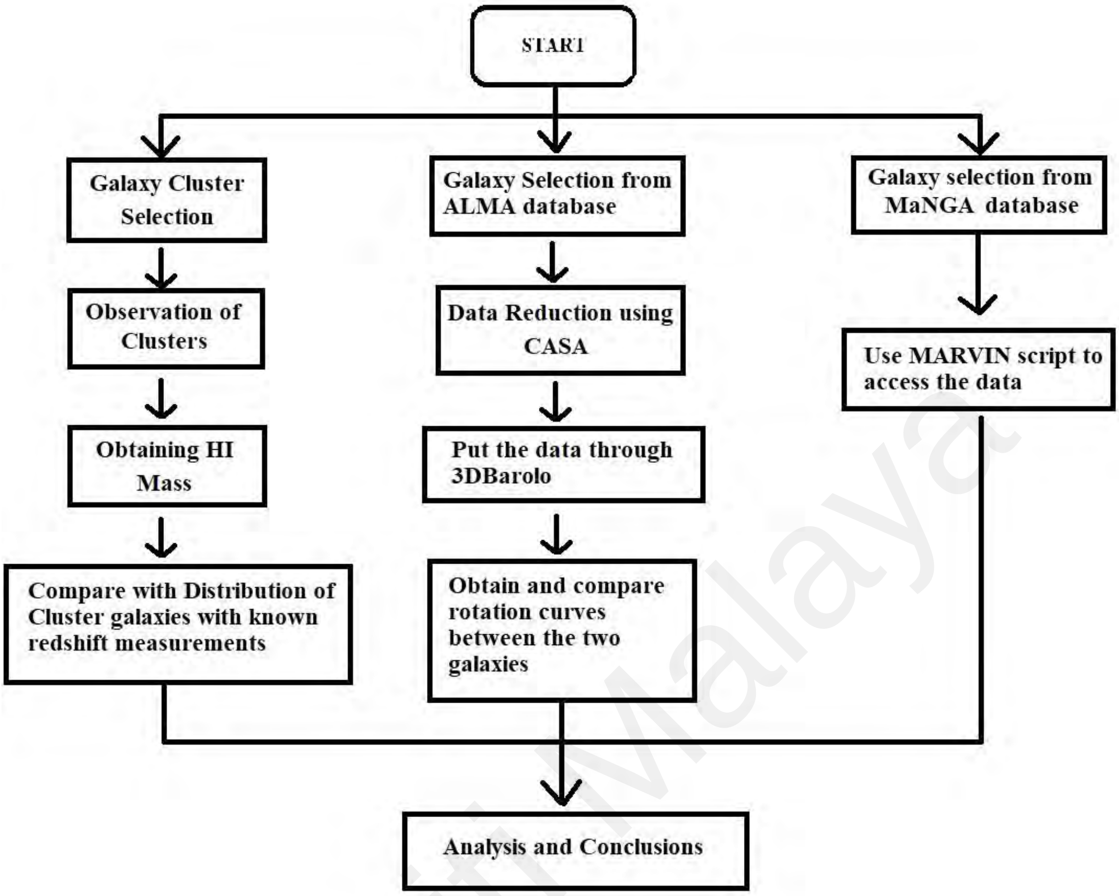

Figure 3.3: The flow chart of this thesis.

CHAPTER 4: DATA REDUCTION

4.1 Data Reduction of HI Data

The data reduction was carried out with the software called DRAWSPEC. DRAWSPEC is a software designed by Harvey Liszt for data reduction of single dish radio telescopes at National Radio Astronomy Observatory (NRAO). The raw data files from the data recorder of the telescope comes in the ASCII format. DRAWSPEC also has the capability to then convert this into the proprietary DRW file format for further processing. However, this step needs to be done manually.

Next, the remaining scans were then separated into their baseline patterns. Once a pattern is chosen, the scans with the pattern were then selected to be further cleaned (i.e. removing the 'spikes' and 'peaks' in the scans). In addition, the scans must also be calibrated by using what is known as the scaling factor. To obtain this parameter, the radio telescope was first used to observe a 'standard radio source'. This source is basically an astronomical object whose flux density has been standardized at a particular value. In this case, the source chosen was Cygnus A. The flux density set by the NRAO was 1621 Jy at 1420 MHz.

The individual scans were not necessarily scaled correctly when first obtained. Thus, it is again important to rectify this. In this case, the standard source used was region S7. In the paper of Williams et al. (1973), Region S7 has the coordinates of R.A.(J2000): 02h 06m 12.0s, Dec.(J2000): 60deg 33m. The peak of S7 was given as 100K. The individual scans were then rescaled as appropriate.

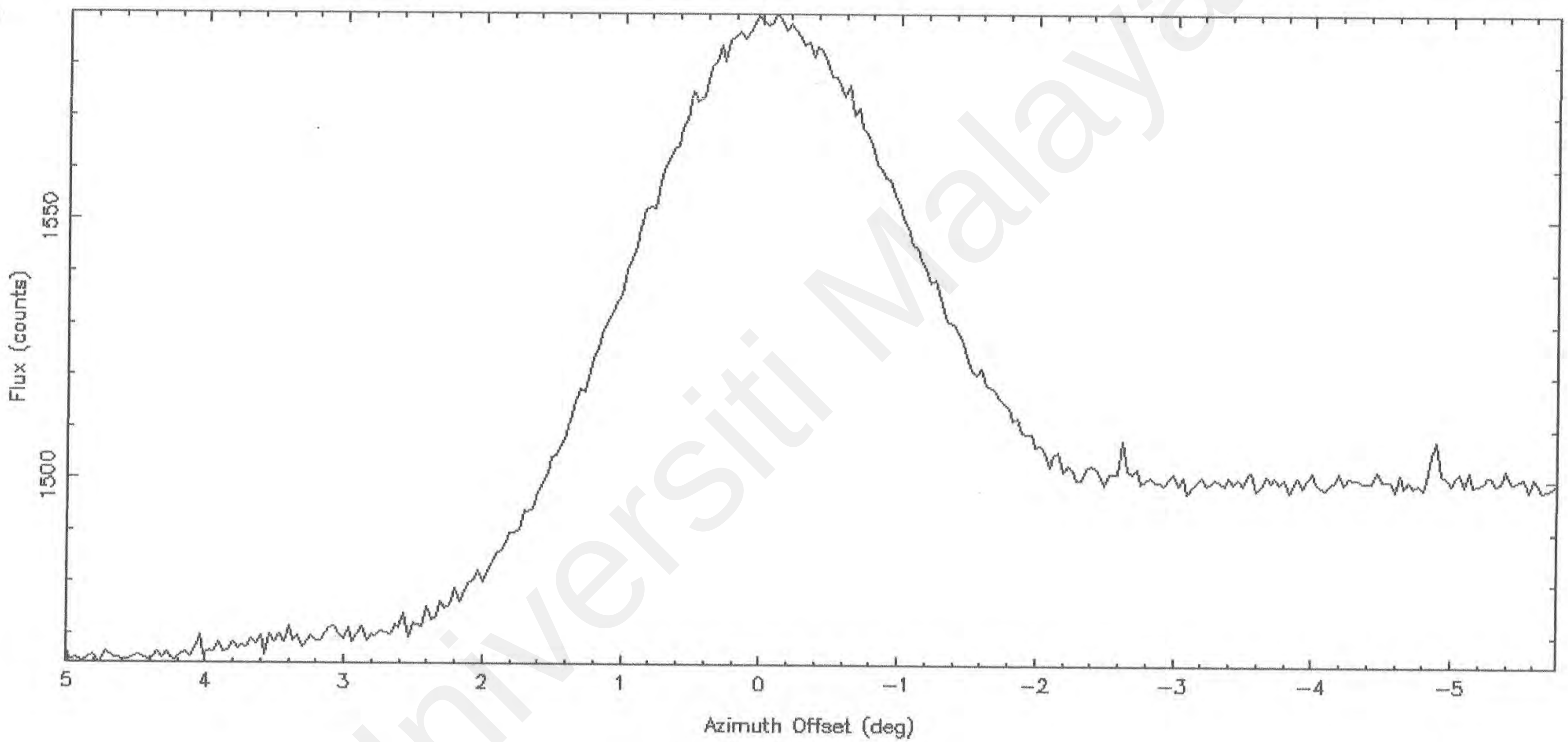

Figure 4.1 The sample spectrum of Cygnus A.

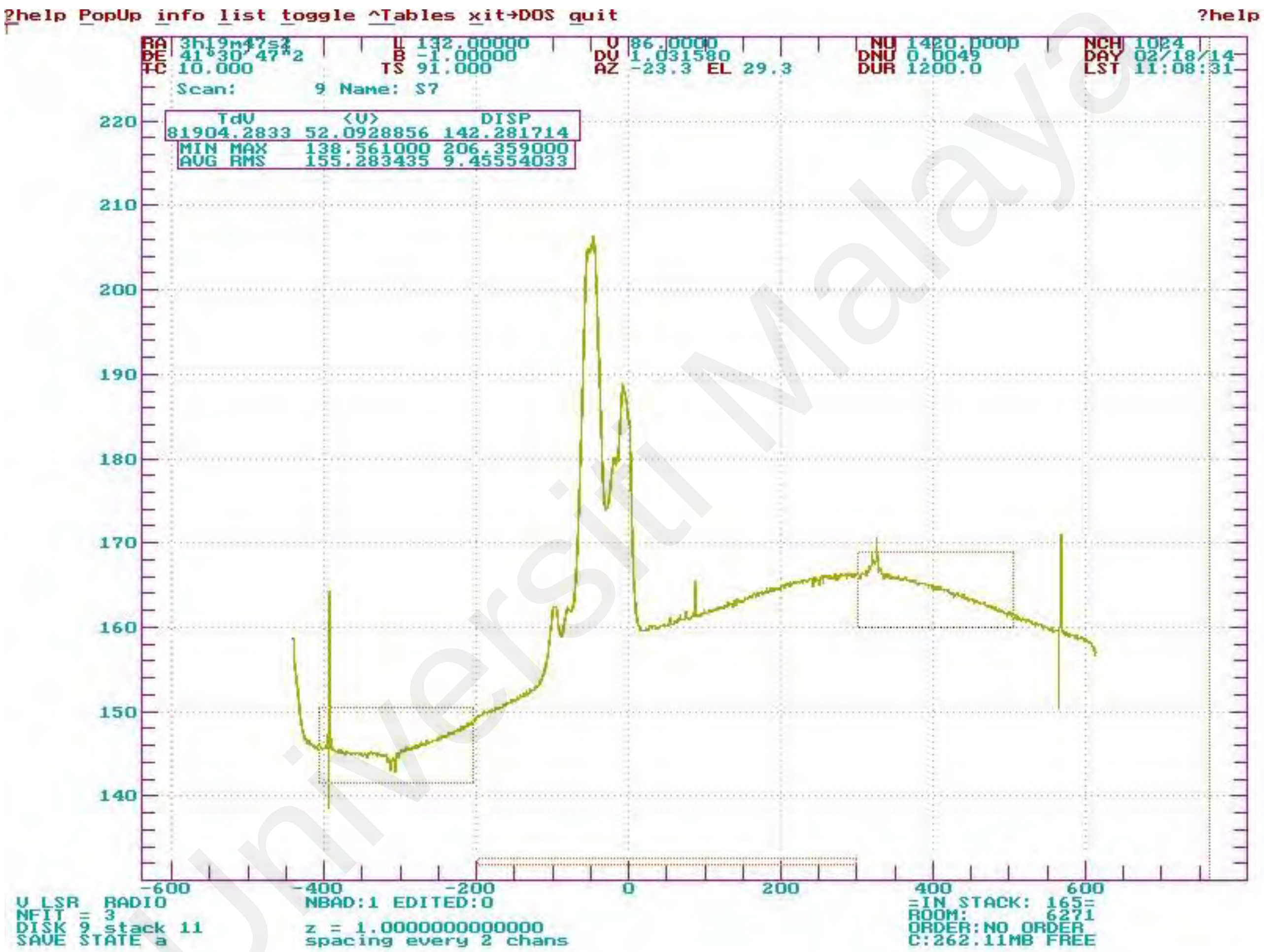

Figure 4.2 The sample spectrum of the Region S7. This image was also intended to illustrate the DRAWSPEC Software User Interface.

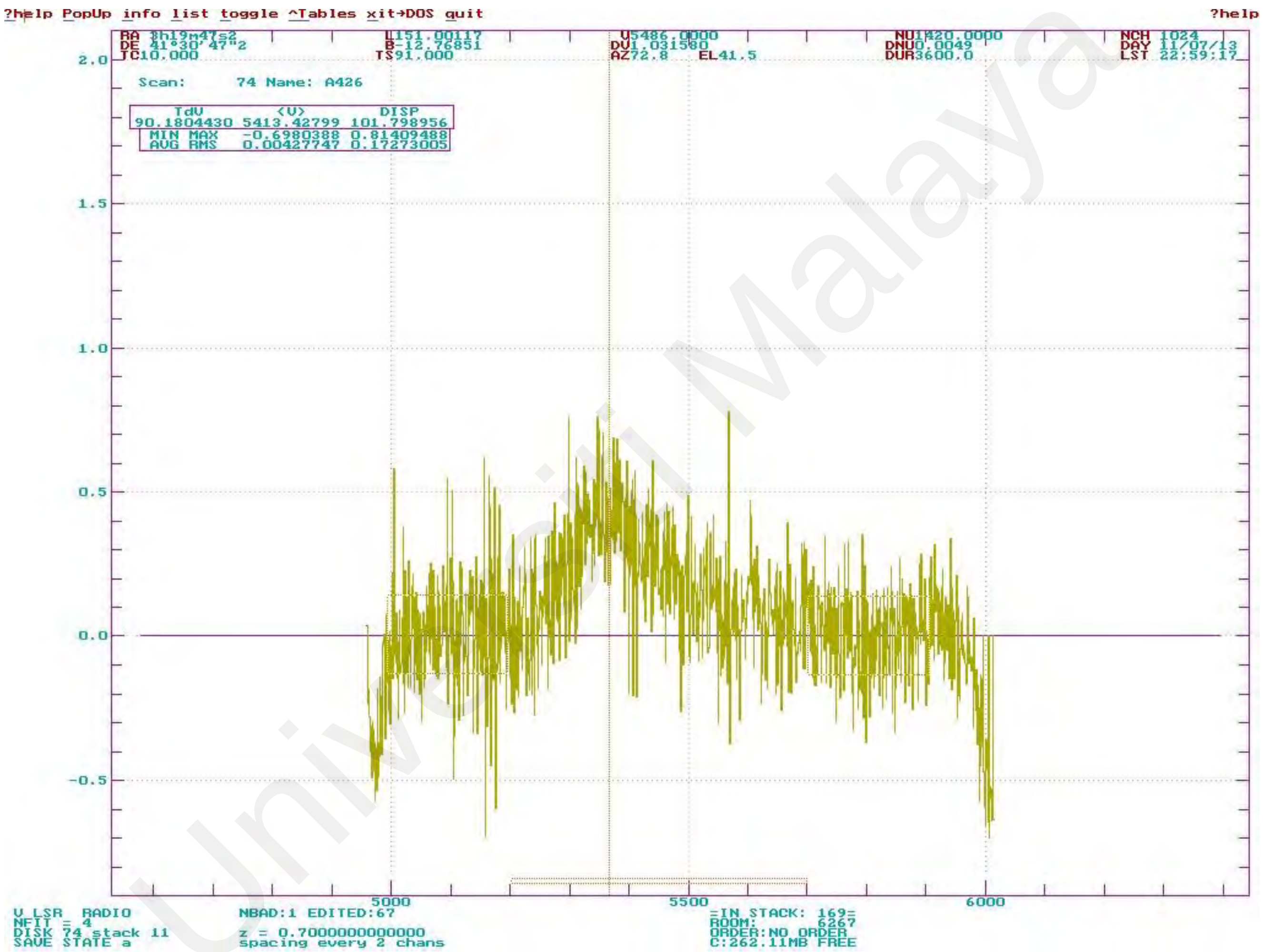

Figure 4.3 An example of a scan that has been baselined and calibrated. In this case, it is for the cluster A426.

Once all the scans have been processed, they were then stacked. The area under the curve was then integrated. The final stacked scan will assist in calculating the mass of HI by providing the flux density integral to be used in the equation 4.1 from Roberts (1962):

$$Mass\ of\ HI = 2.36 \times 10^5\ \times D^2\ x \int S_v\ \ dv \qquad (4.1)$$

Where D is the distance to the cluster in Megaparsecs, while $\int S_v dv$ is the flux density integral in Jy km s^{-1}.

The following step in this part is to compare the number of galaxies with the HI spectra obtained to see whether the detected HI originates from the galaxies in the cluster. Data for the individual cluster galaxies was obtained from the NASA Extragalactic Database (NED).

4.2 Data Reduction of CO (3-2) Data

The data for the galaxies were reduced by using the Common Astronomy Software Application (CASA). The scripts to reduce the data (including calibration) were included in the download. CASA only works on Unix language machines. The scripts supplied together with the raw data will result in a generation of FITS file.

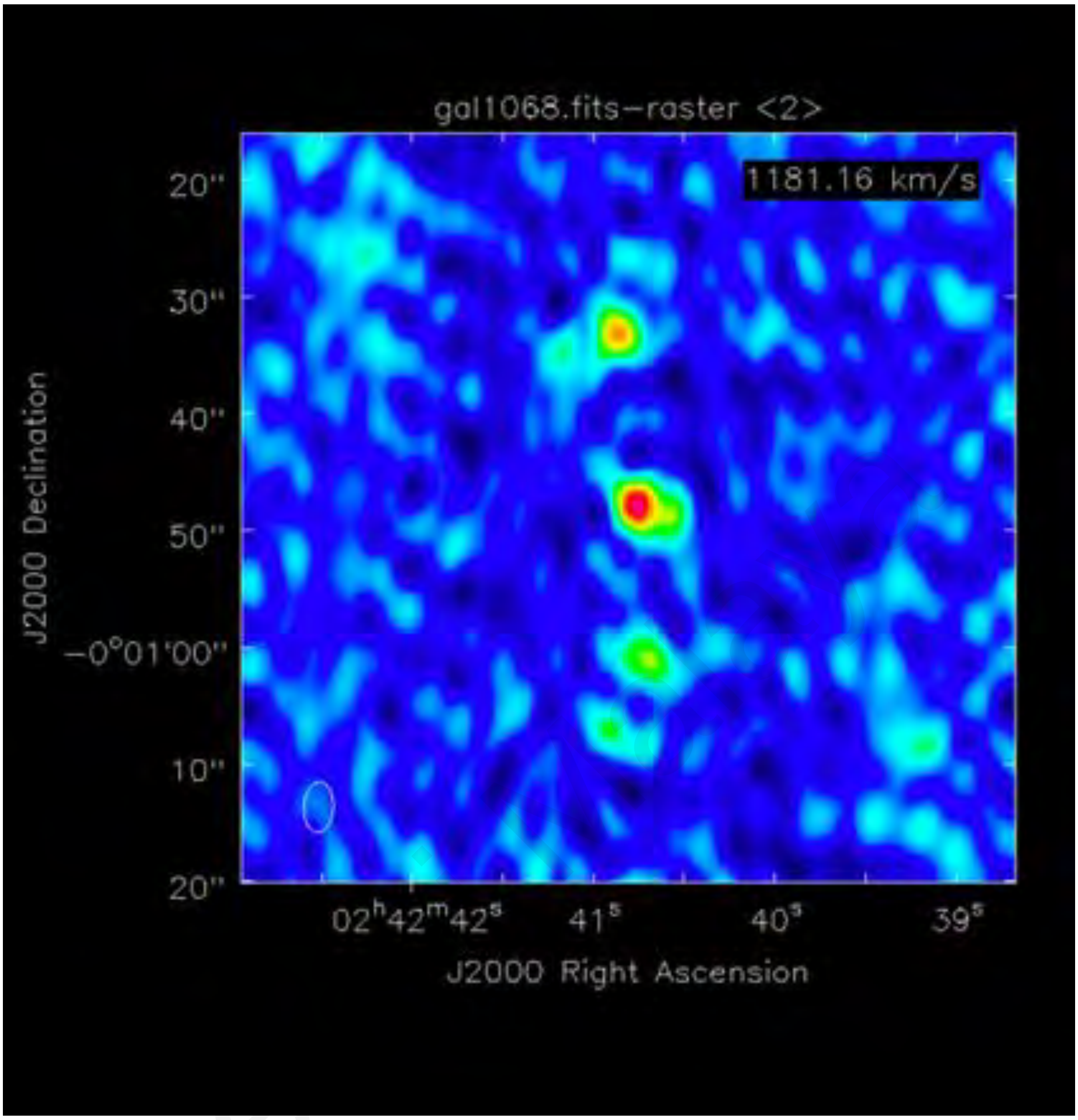

Figure 4.4: The FITS file image for NGC 1068

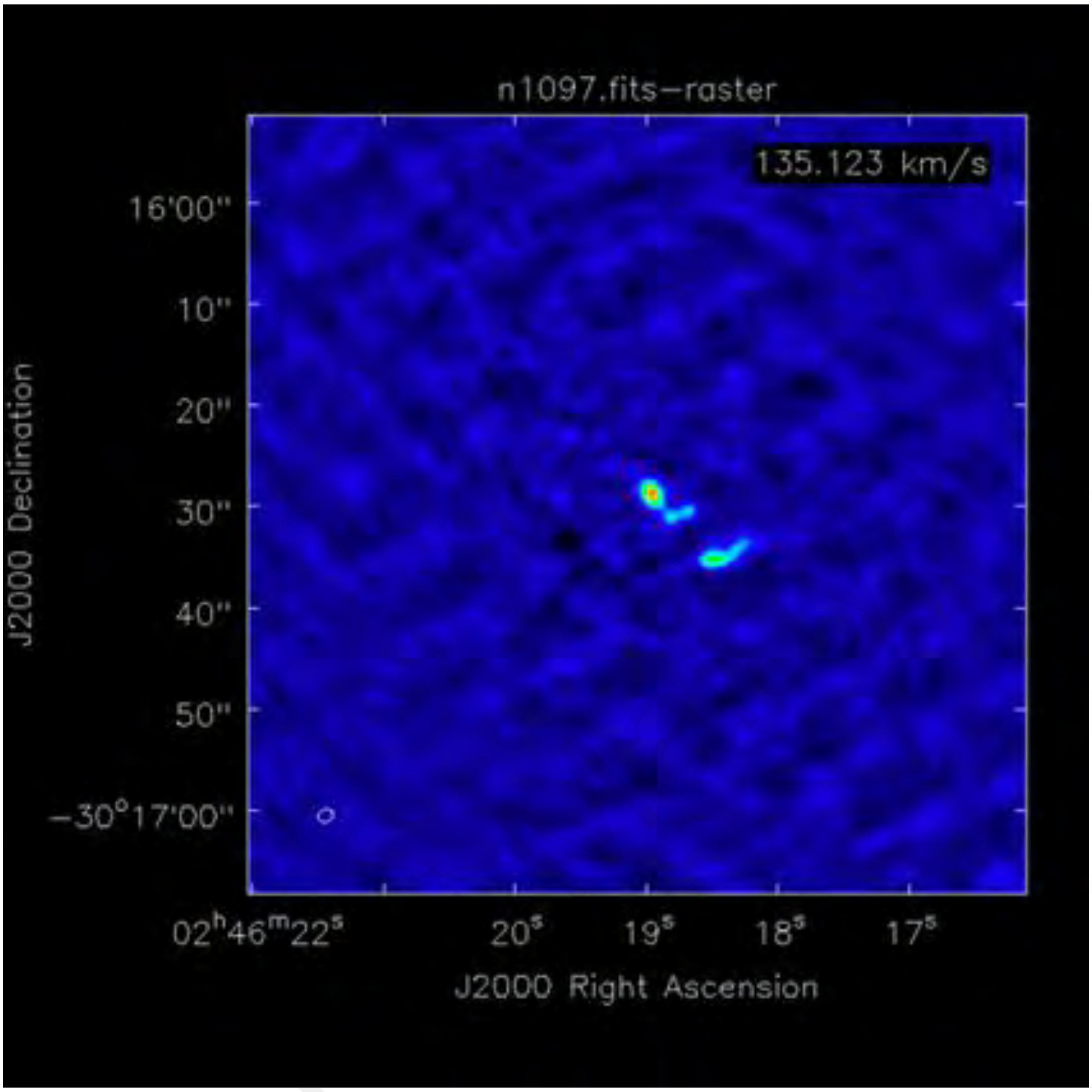

Figure 4.5: The FITS file image for NGC 1097.

Once the FITS file were obtained, the images were then run through a software called 3DBarolo (3D-Based Analysis of Rotating Object via Line Observations). This software was developed by Enrico M. Di Teodoro and Filippo Fraternali to fit 3D tilted ring models to data cubes of emission-lines (Terodo & Fraternali,2015).

The broad purpose of 3DBarolo is to find the kinematics of any disk-like objects. In our case, it is used to help derive the rotation curve for NGC 1068 and NGC 1097 especially the position angle parameter. This software requires the input parameters such as the inclination angle and systemic velocity of the galaxie to work properly.

These parameters were inputted into a parameter file that was then read by the software. The output from 3DBarolo was the used in generating the PV diagram for both galaxies.

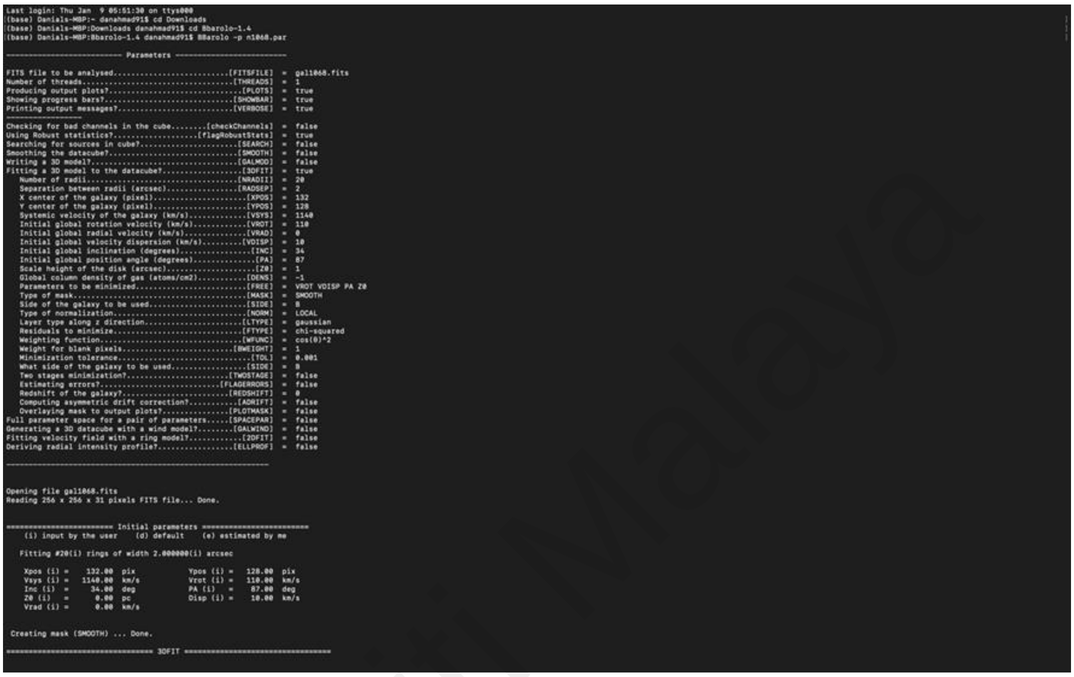

Figure 4.6: An example of the 3DBarolo software running.

For the MaNGA data, the script used was ran on Google Colaboratory. The output is a series of velocity maps of Hydrogen Alpha. The HI spectra corresponding to these galaxies were obtained directly from the DR15 online database via the link: https://dr15.sdss.org/sas/dr15/manga/HI/v1_0_1/spectra/GBT16A_095/ascii/. The spectra were plotted using Python.

CHAPTER 5: RESULTS AND ANALYSIS

The results section is split into galaxy cluster scale and galaxy scale results.

5.1 Galaxy Cluster Observations

Results from the stacking of the scans have indicated that the mass of HI was calculated to be (3.2 $\pm$ 0.4) x 10^{10} solar masses. For comparison purposes, the M_{HI} of A1367 was found to be (1.6 $\pm$ 0.4) x 10^{11} solar masses from the HI line intensity of 54.3$\pm$25.2 Jy kms^{-1}. The binned spectrum of A426 is shown in Figure 4.3. The redshift distribution was also carried out for the galaxies within the beam size of the telescope. The error bars in Figures 5.1 and 5.2 were from the root mean square (rms) signal of the telescope itself.

The detected CO emission in the Brightest Cluster Galaxy of A1367 implies a smaller total molecular gas mass (2.4 $\pm$ 0.5 x 10^{8} solar masses, Edge (2001)) but very different dynamics in centroid and line width (Lim et al. 2000). At face value this implies a ratio of HI to H_2 of ~ 650, although the HI detection may be related to a much larger mass of atomic gas away from the central galaxy and much more cold molecular gas that is as yet unaccounted for. There is also a list of dwarf galaxies that have been detected in the same part of the sky as the cluster by past surveys (Conselice et al. 2003). Some of the dwarfs discovered are confirmed to be background objects. However, there are many more that do not have confirmed membership status. In an effort to give some relation of the HI mass discussed here, the mass of HI of two other galaxy clusters were compared with.

Also, in Figures 5.1 and 5.3, there is a distinctive “knee” in the HI profile of A426 at approximately 5600 km/s. This coincides with an increase in the number of late-type galaxies in this velocity bin. The increase in the number of late-type galaxies are linked with the increase in HI detection.

Figures 5.3 and 5.4 shows that the distribution of galaxies with known redshifts is much broader than the HI Spectra obtained. This might be an indication that many galaxies in both clusters are actually deficient in HI. This is especially for A1367, which is a known case of an on-going cluster merger. Further explanation of this is has been covered in Chapter 2 Section 2.1.1.

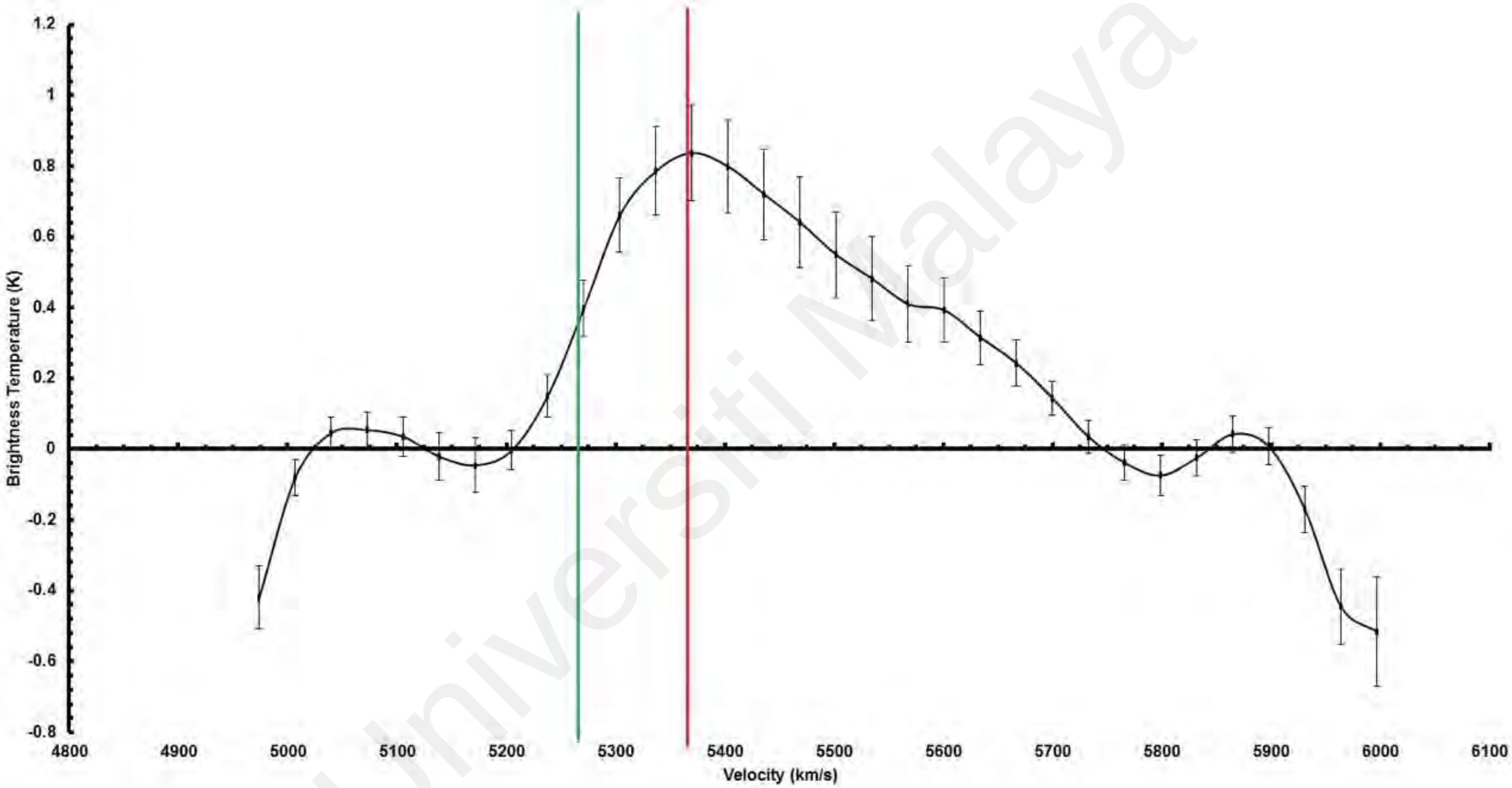

Figure 5.1: The Stacked HI Spectra of Abell 426. The green line marks the velocity of the central galaxy NGC 1275, while the red line indicates the average velocity of the cluster at 5366 kms^{-1} .

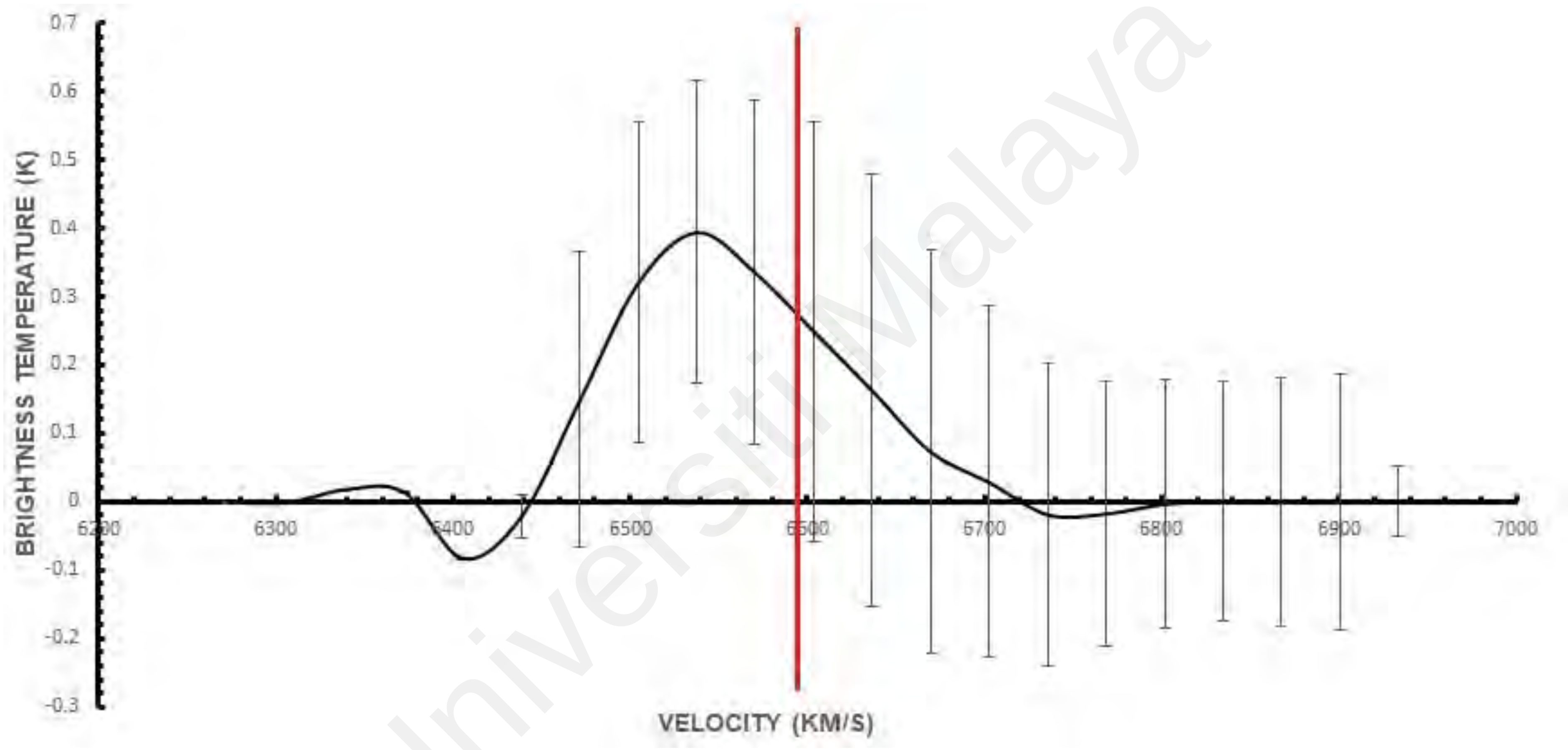

Figure 5.2 The Stacked HI Spectra for A1367. The red line indicates the average velocity of the cluster at 6595 kms^{-1}.

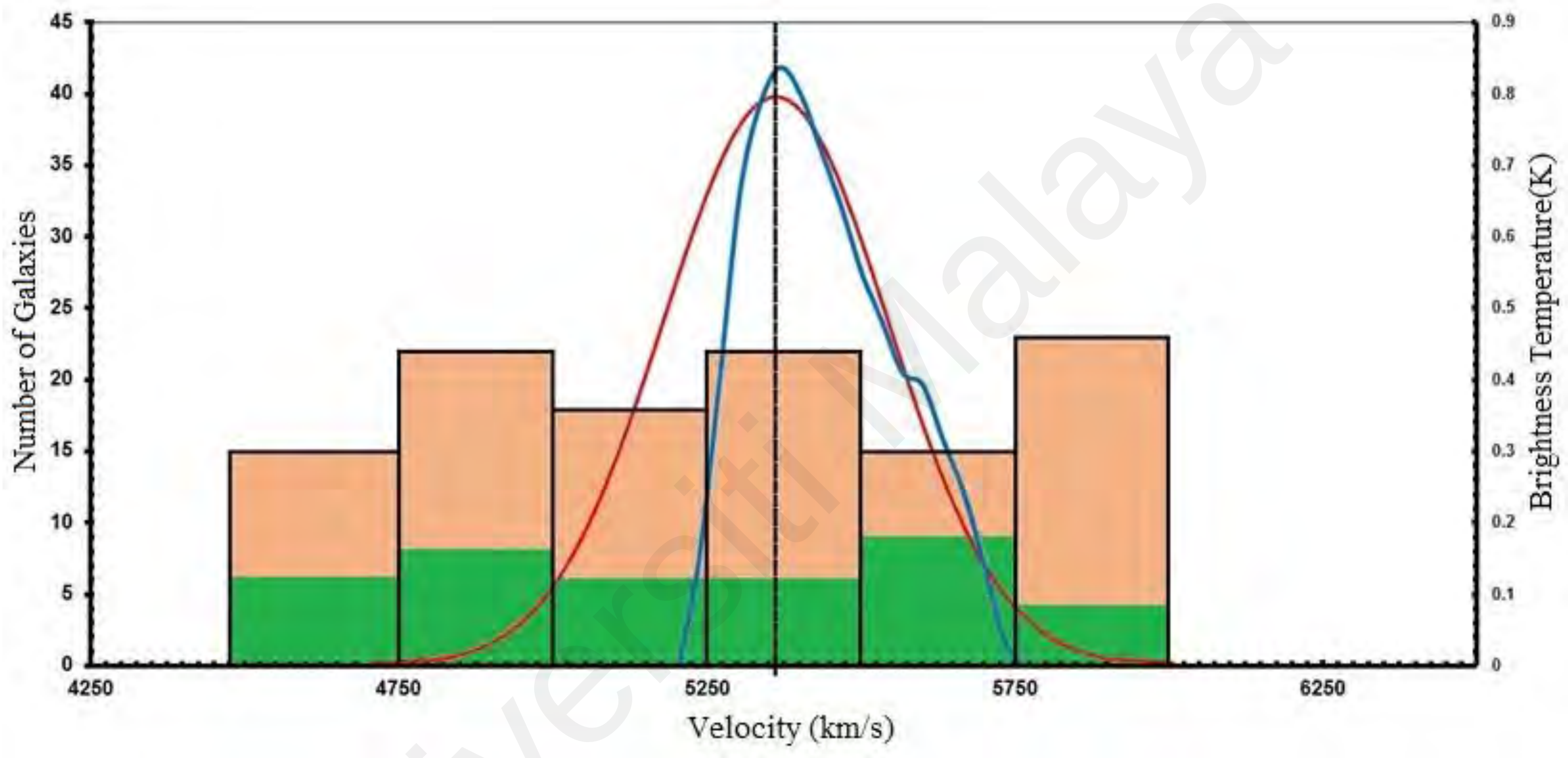

Figure 5.3: The velocity histogram for A426 for the galaxies that are in the beam of the telescope. The green portions of the bars indicate the spirals. The Red Gaussian line shows the idealized distribution. The blue line shows the HI brightness temperature of HI as shown in Figure 5.1.

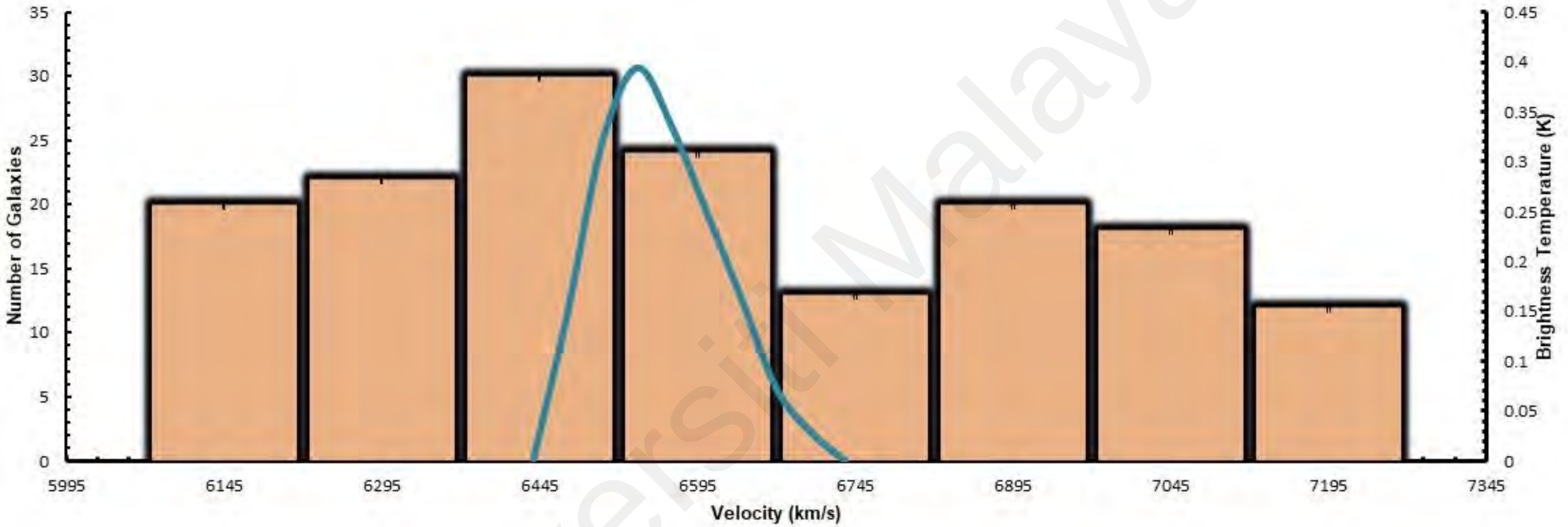

Figure 5.4: The histogram of Galaxies for A1367 superimposed with the HI spectra (blue line) of the cluster as obtained in Figure 5.2.

Table 5.1: The table of galaxy clusters of similar richness and roughly similar redshift. This is the sum of the mass of HI in the individual galaxies of the respective cluster. The value for the Virgo cluster was obtained from Davies & Lewis (1973) while the value for the Fornax cluster was from Schroeder et al. (2001). The value for Abell 370 comes from Lah et al. (2009)

Name of Cluster	Mass of HI (Solar Masses)
Virgo Cluster	6.1×10^{10}
Fornax Cluster	2.1×10^{11}
Abell 370	6.6×10^{9}

5.2 Galaxy Scale Observations

The results from the 3DBarolo fitting are in Figures 5.5 and 5.6.

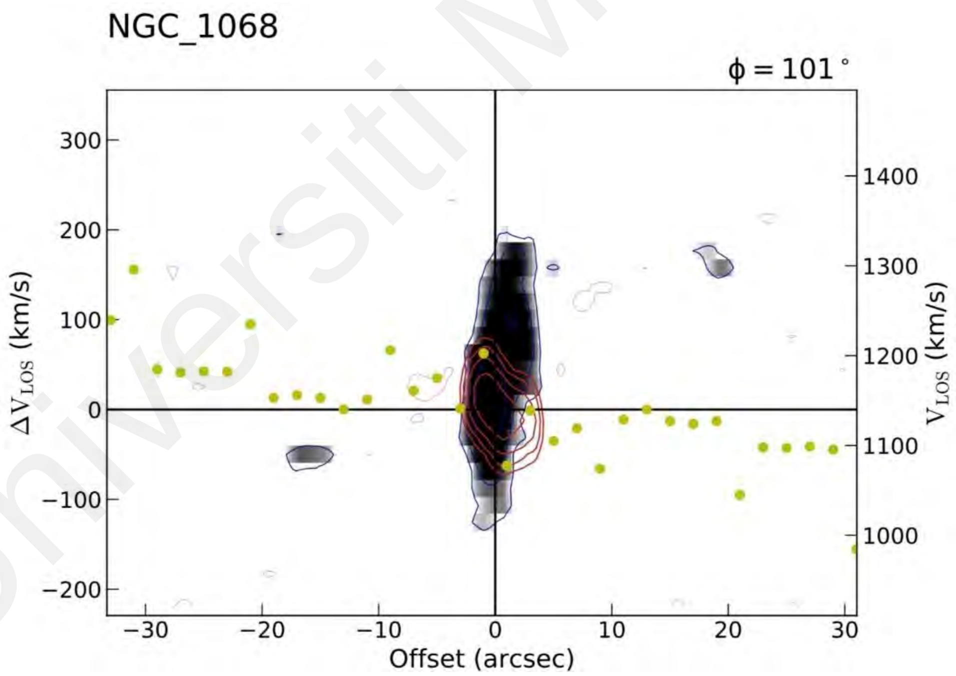

Figure 5.5: The fitting results for NGC 1068 with the 3DBarolo software. The position angle given is 101 degrees.

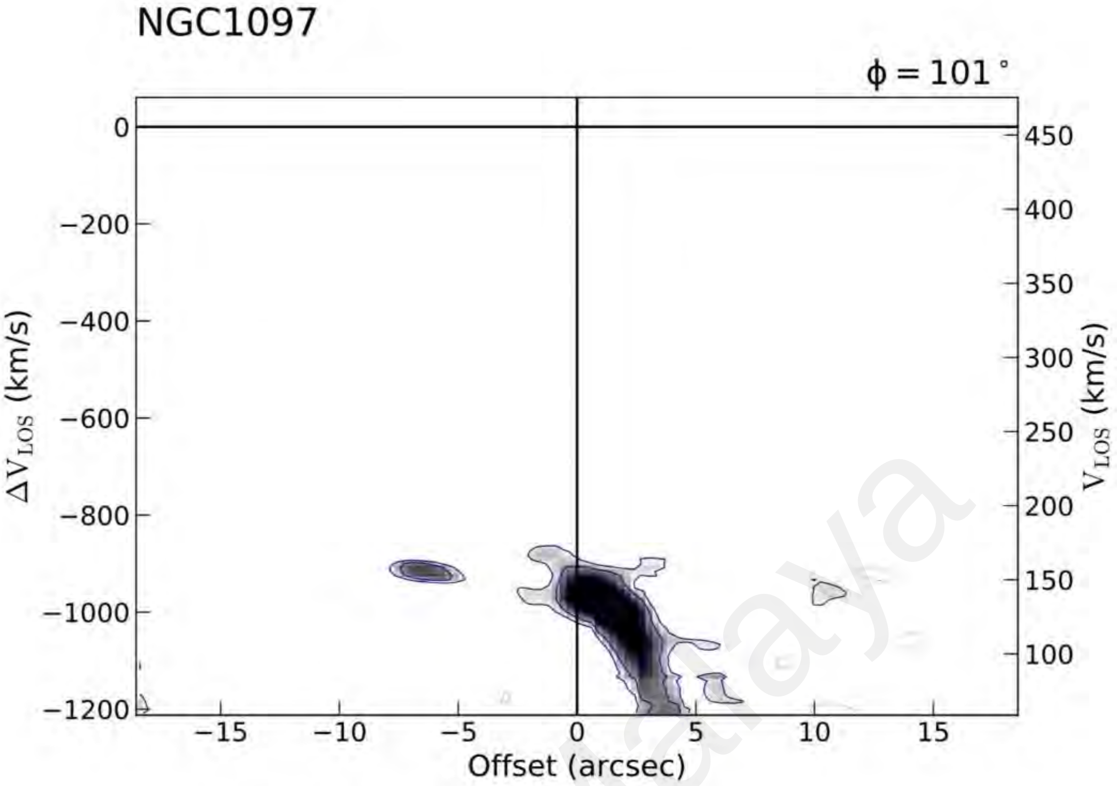

Figure 5.6: The results for NGC 1097. The position angle given is 101 degrees.

Following on from this, the Position Angle for both galaxies were used to obtain the following rotation curves in Figure 5.7 and 5.8.

By comparing Figures 5.7 and 5.8, it can be seen that the velocity of CO starts to rise sharply. However, at a radius of 0.2 kpc for NGC 1068, the increase in rotation velocity starts to drop slightly in comparison to the increase in the same radius for NGC 1097. Note also, in Figure 5.7, the “knee” in the plot of the rotation curve at radius of ~ 1.5 kpc. Note also that the rotation curve of NGC 1097 starts to straighten out at 230 km/s, compared to 140 km/s for NGC 1068.

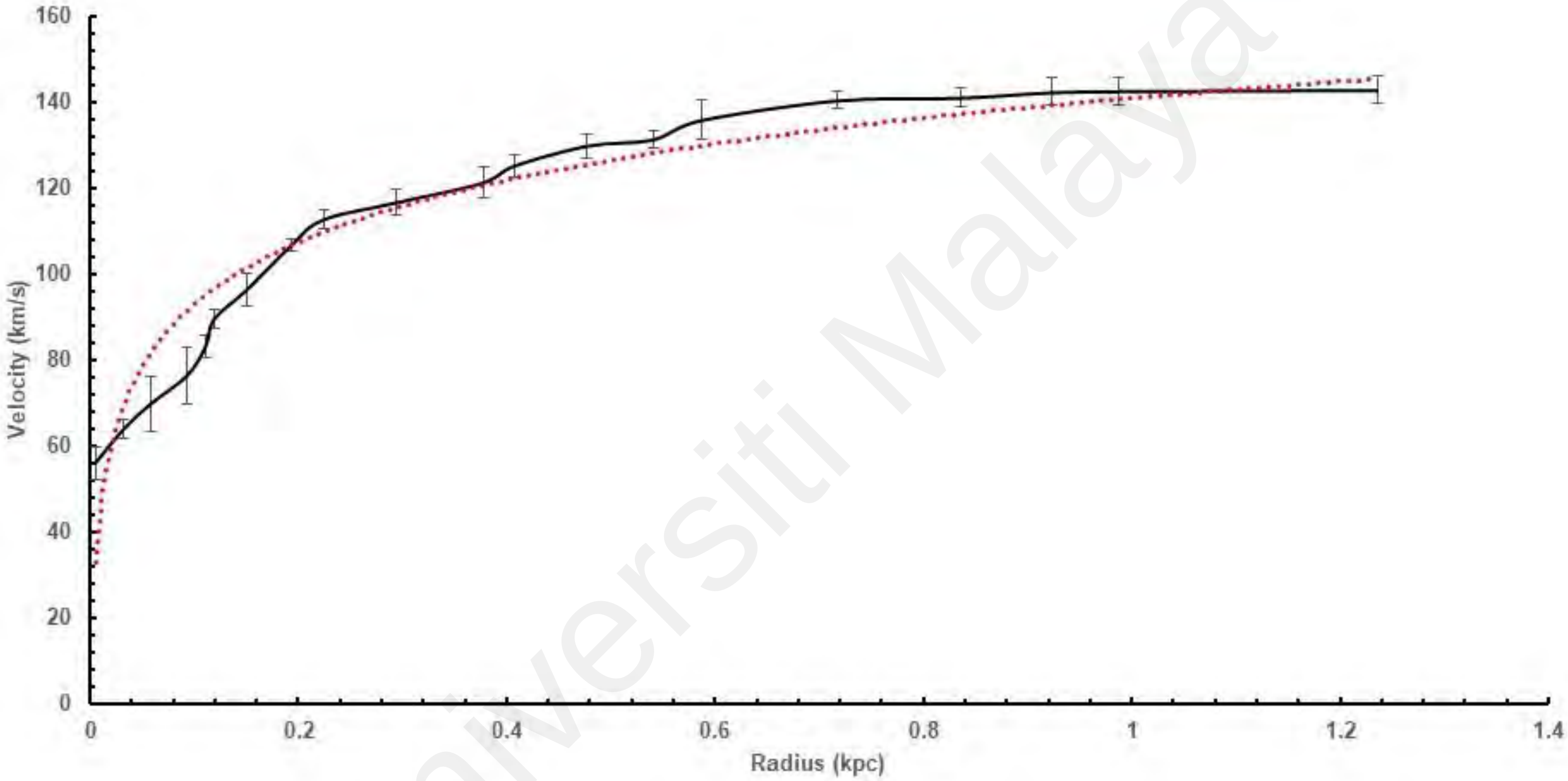

Figure 5.7: The rotation curve of NGC 1068. The red dotted line is the modeled fit.

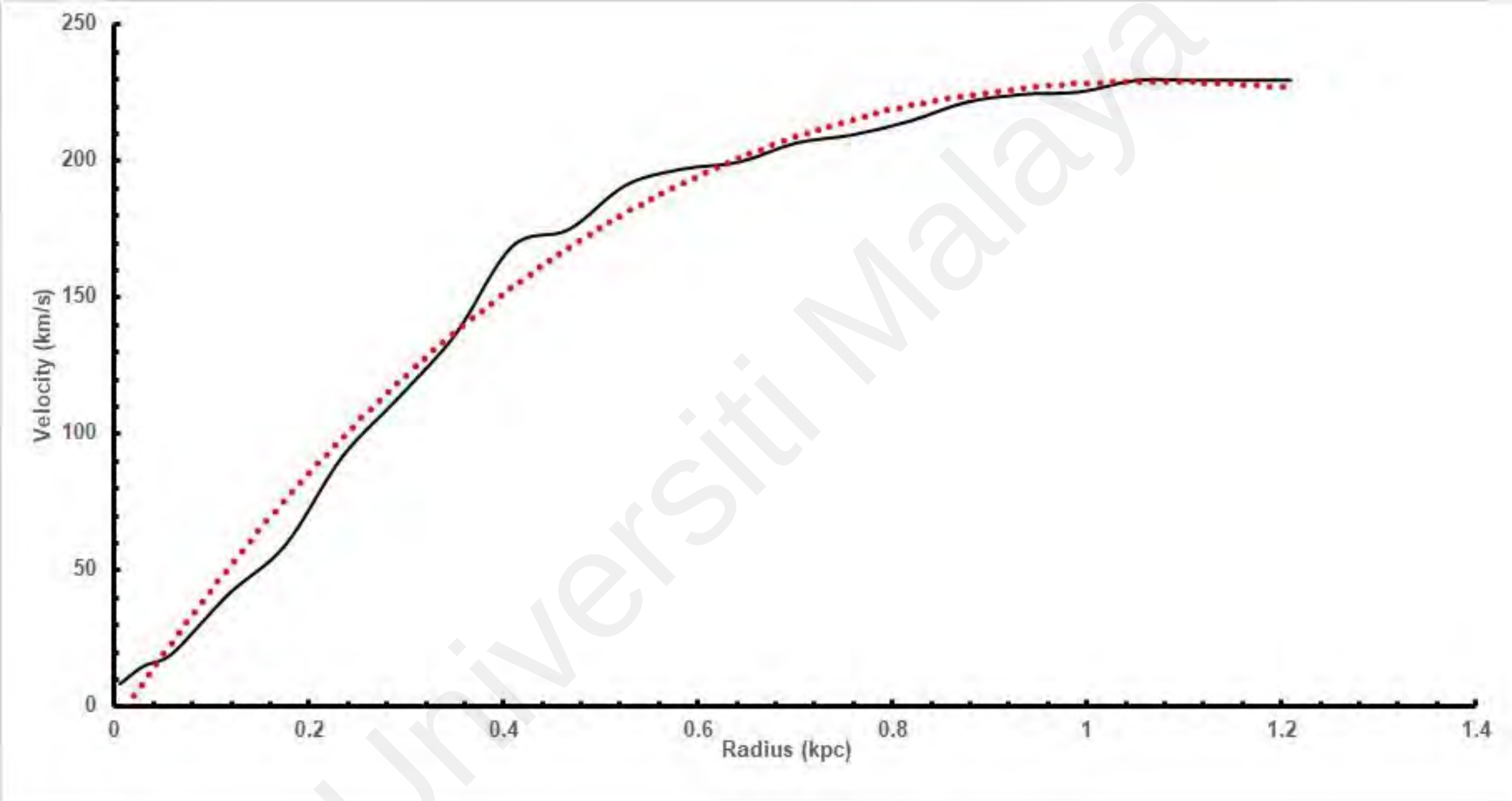

Figure 5.8: The rotation curve of NGC 1097. As in Figure 5.7, the red dotted line is the modeled fit.

It is possible that this behavior could be attributed to a case or a minor merger in NGC 1068's past. Previous studies such as Tanaka et al. (2017) have highlighted certain features that point to a minor merger event. However, depending on when the merger event happens, the dynamics of the galaxy should be starting to reach equilibrium now, as NGC 1068 is not currently interacting with any visible companion. For the case of NGC 1097, Higdon & Wallin (2003) suggested that the optical jets are the result of a minor merger incident with a dwarf galaxy. NGC 1097 also has two known companions, NGC 1097A and NGC 1097B, with NGC 1097A currently interacting with NGC 1097. The velocity at the origin of the radius is also much higher for NGC 1068 than it was for NGC 1097. These differences are tentative signs of the characteristics of Compton-thick AGNs.

If we refer to the work of Kalinova et al. (2017), the rotation curves of galaxies can be classified broadly into four types, namely slow-rising, flat, round-peaked and sharp-peaked. For the central 1.2 kpc of the two galaxies, both profiles fit the slow rising category. The Circular Velocity Curves developed by Kalinova et al. (2017) are however applied across the entire galaxy instead of just the central region.

The MaNGA data results are shown in Figures 5.9 to 5.18. Note that the MaNGA IDs of the galaxies are used here. The HI spectra shown has been correctly baselined and calibrated. The GBT observations have a rms of 1.5mJy at 10kms^{-1} (Masters et al. 2019).

The statistical error of the HI flux was calculated by using equation 5.1. (Masters et al. 2019)

$$Error\ in\ HI\ Flux = rms\ \sqrt{\Delta v W} \qquad (5.1)$$

Where Δv is the channel resolution after Hanning smoothing (10 kms^{-1}) and W is the HI profile width.

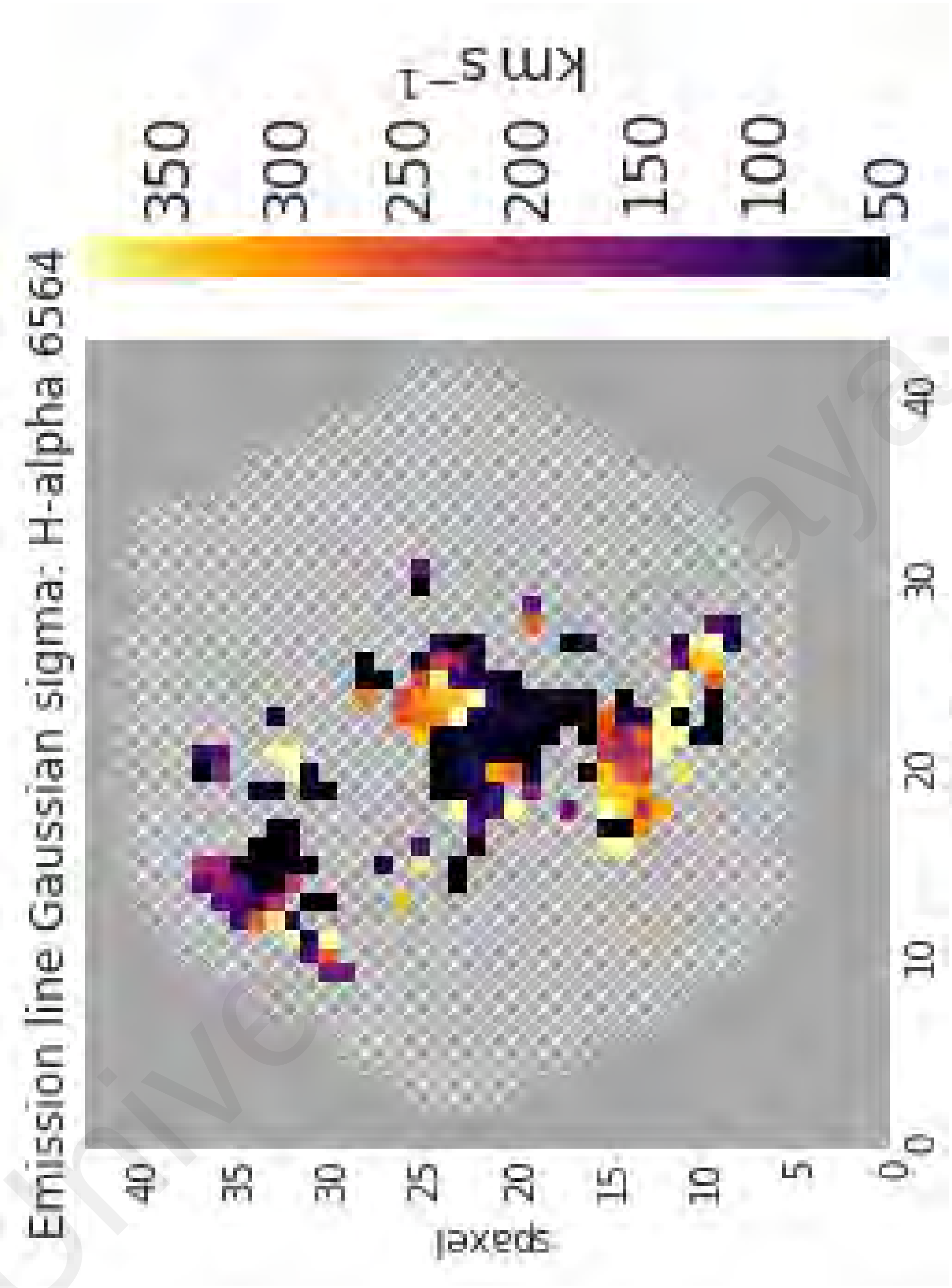
Emission line Gaussian sigma: H-alpha 6564
km s^{-1}
spaxel
spaxel

(a)

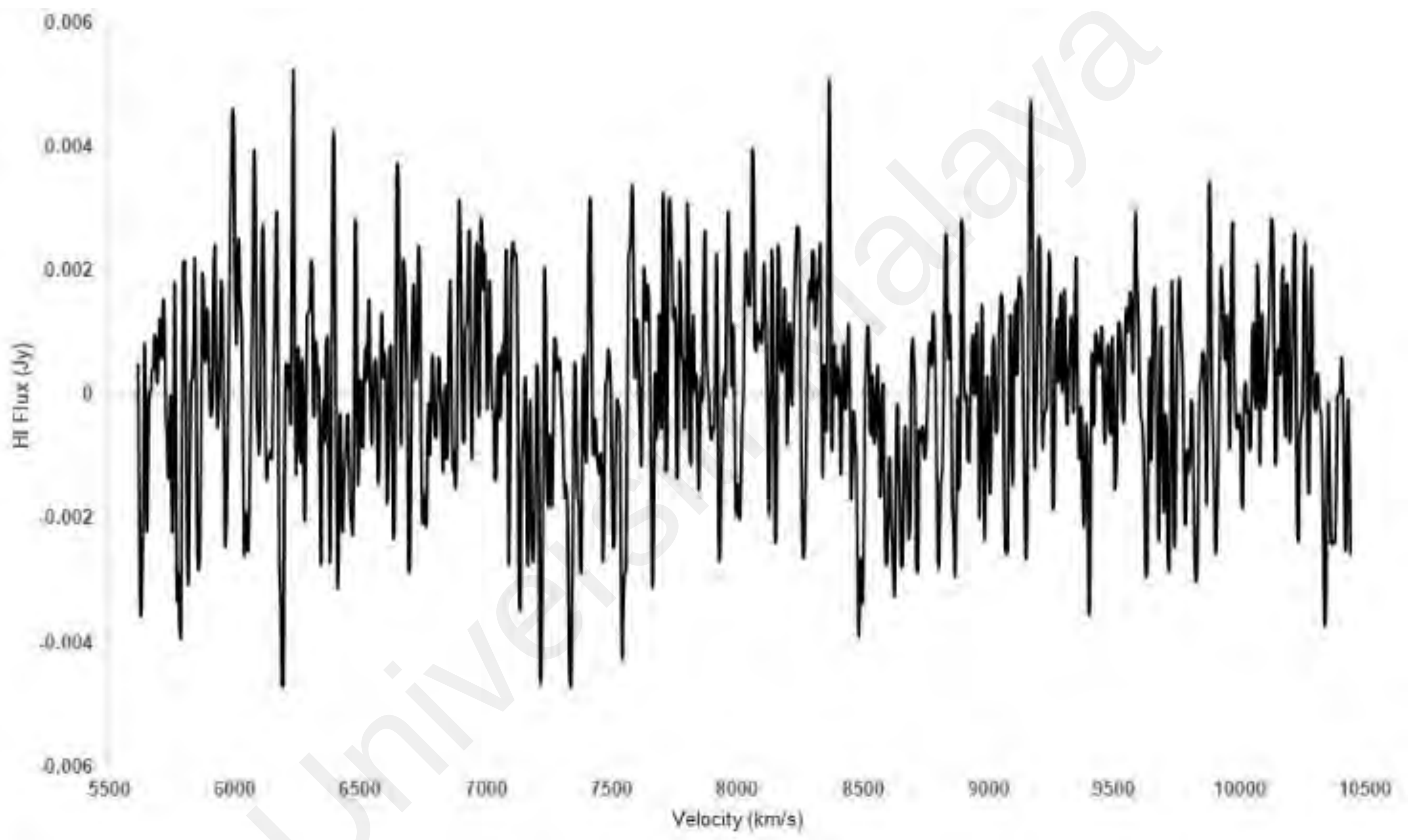

(b)

Figure 5.9: The H-Alpha for the Galaxy 7991-3703 in (a) and the HI spectra of the galaxy in (b). The HI flux error is 332.0 mJy kms^{-1}.

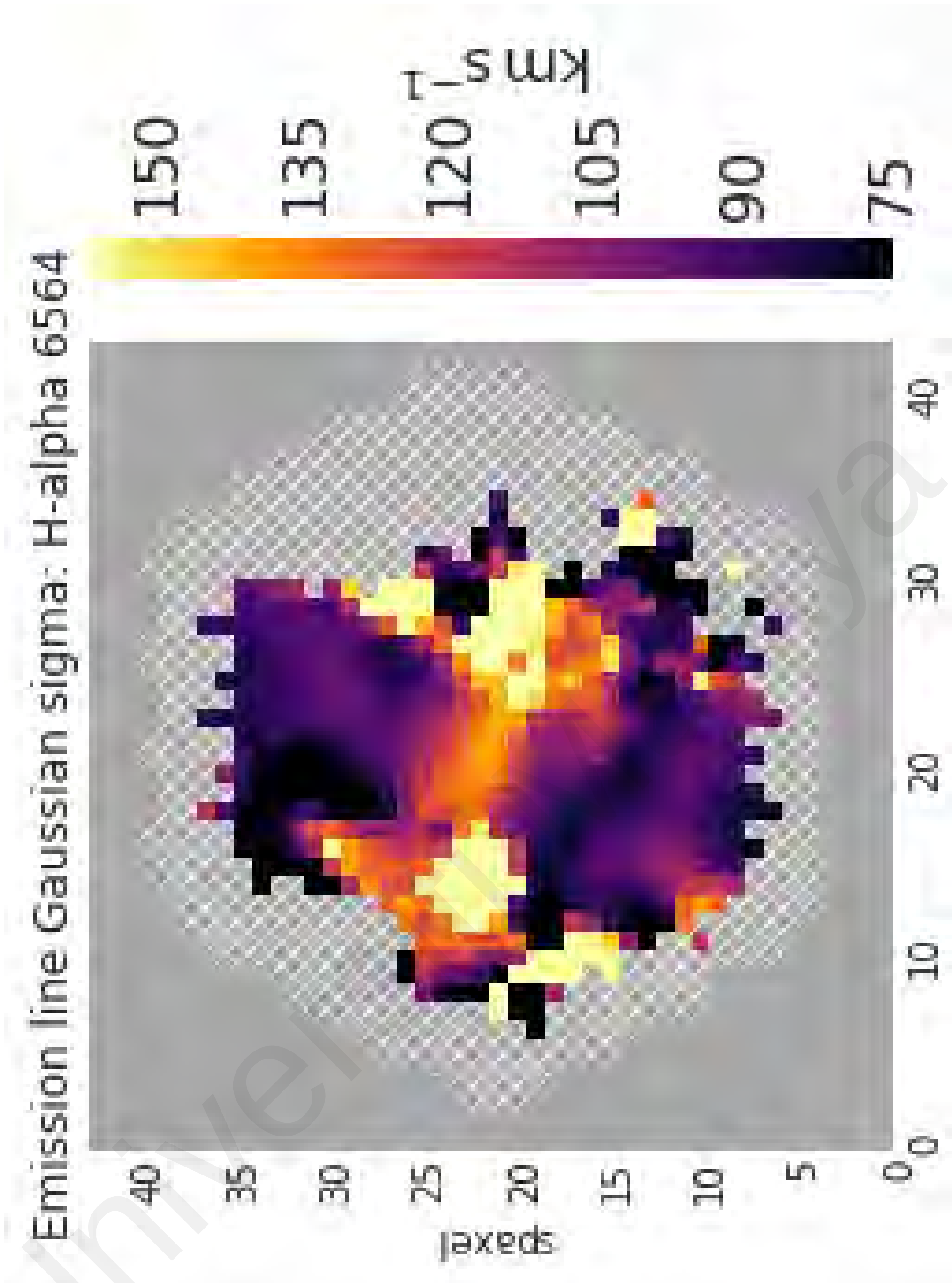

Emission line Gaussian sigma: H-alpha 6564
km s^{-1}
150
135
120
105
90
75
spaxel
spaxel
0
10
20
30
40
0
5
10
15
20
25
30
35
40

(a)

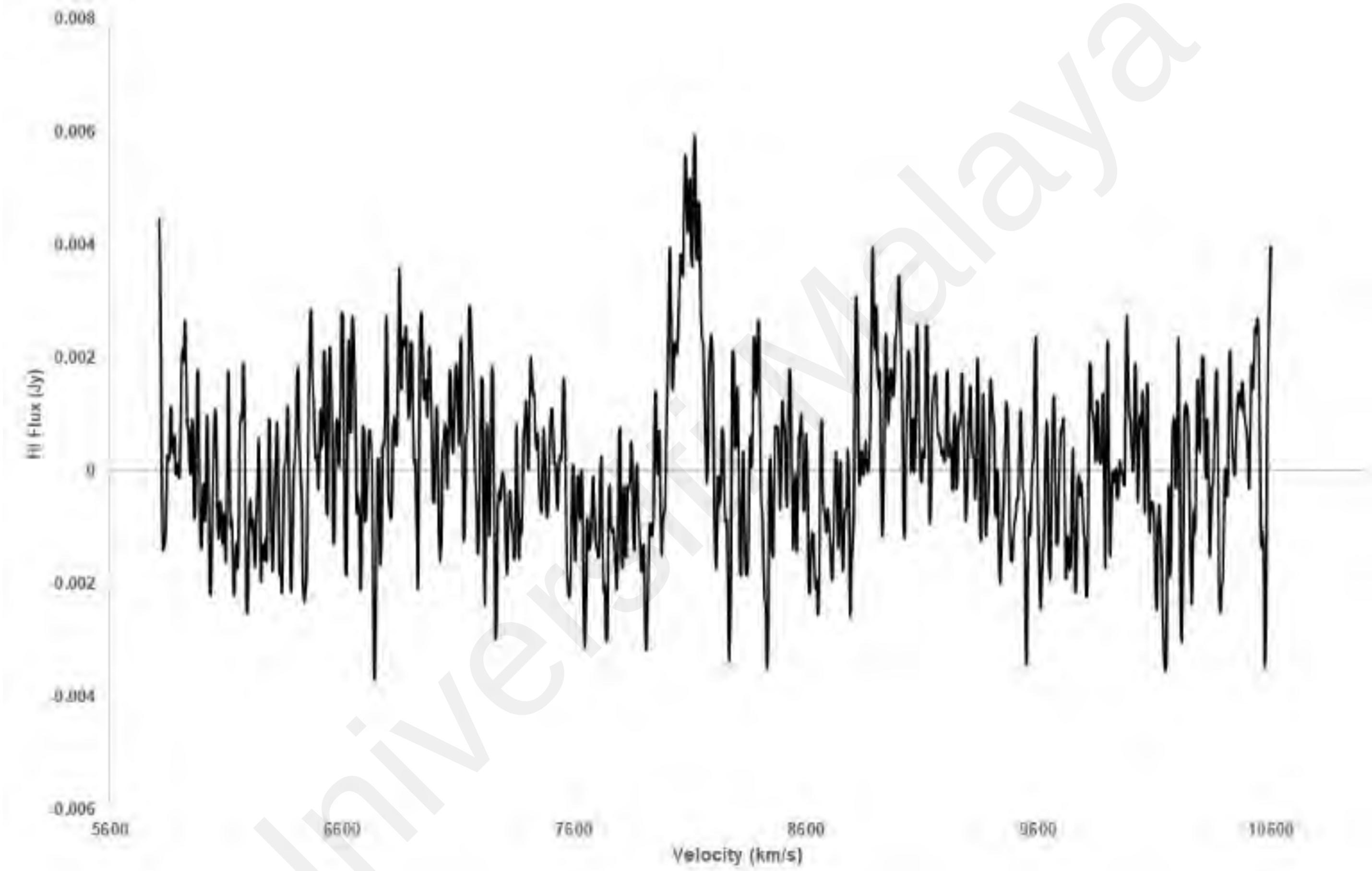

(b)

Figure 5.10: As in Figure 5.9, but for galaxy 7991-3704. The HI flux error is 332.0 mJy kms^{-1}.

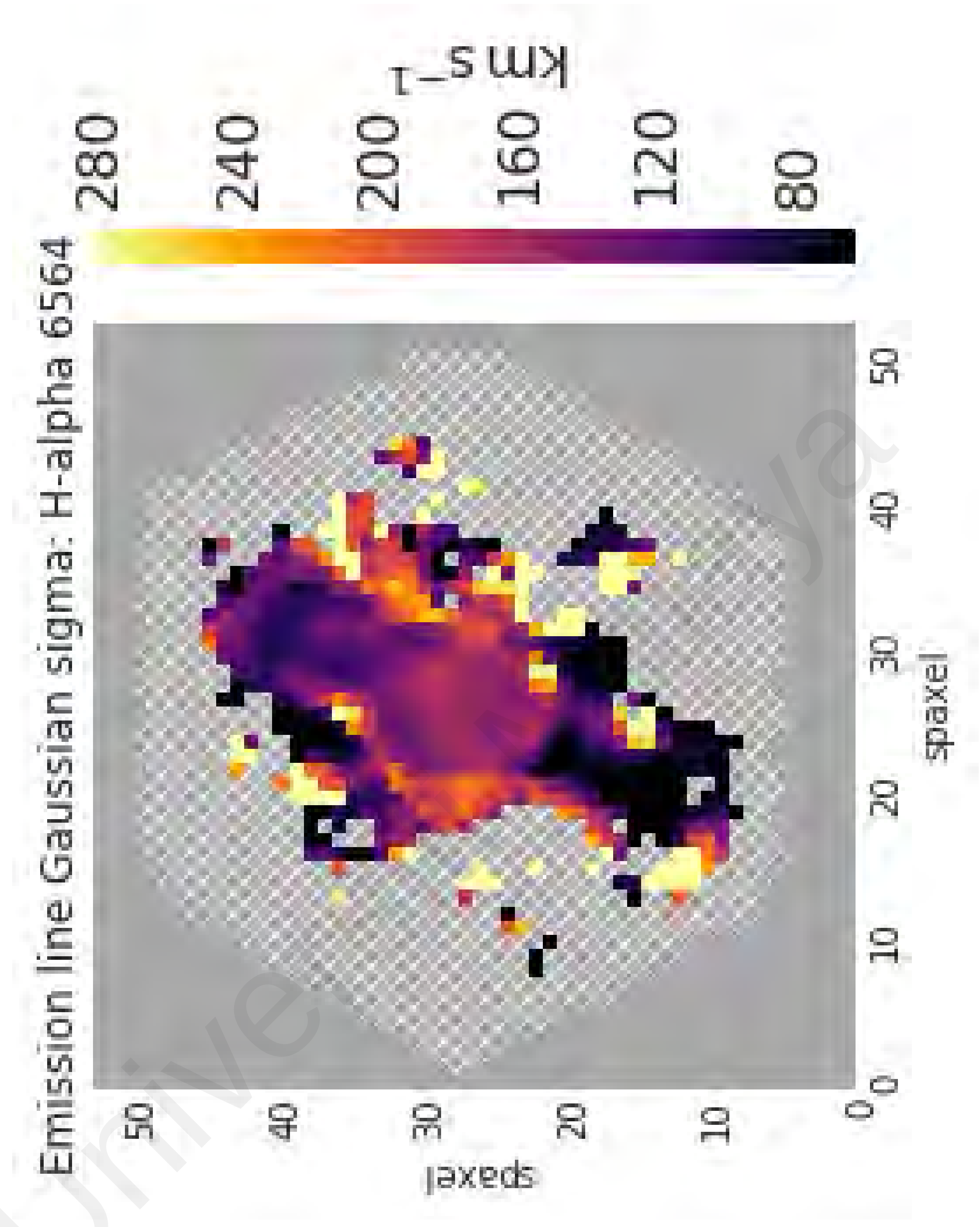
Emission line Gaussian sigma: H-alpha 6564
km s^{-1}
280
240
200
160
120
80
spaxel
spaxel
0
10
20
30
40
50

(a)

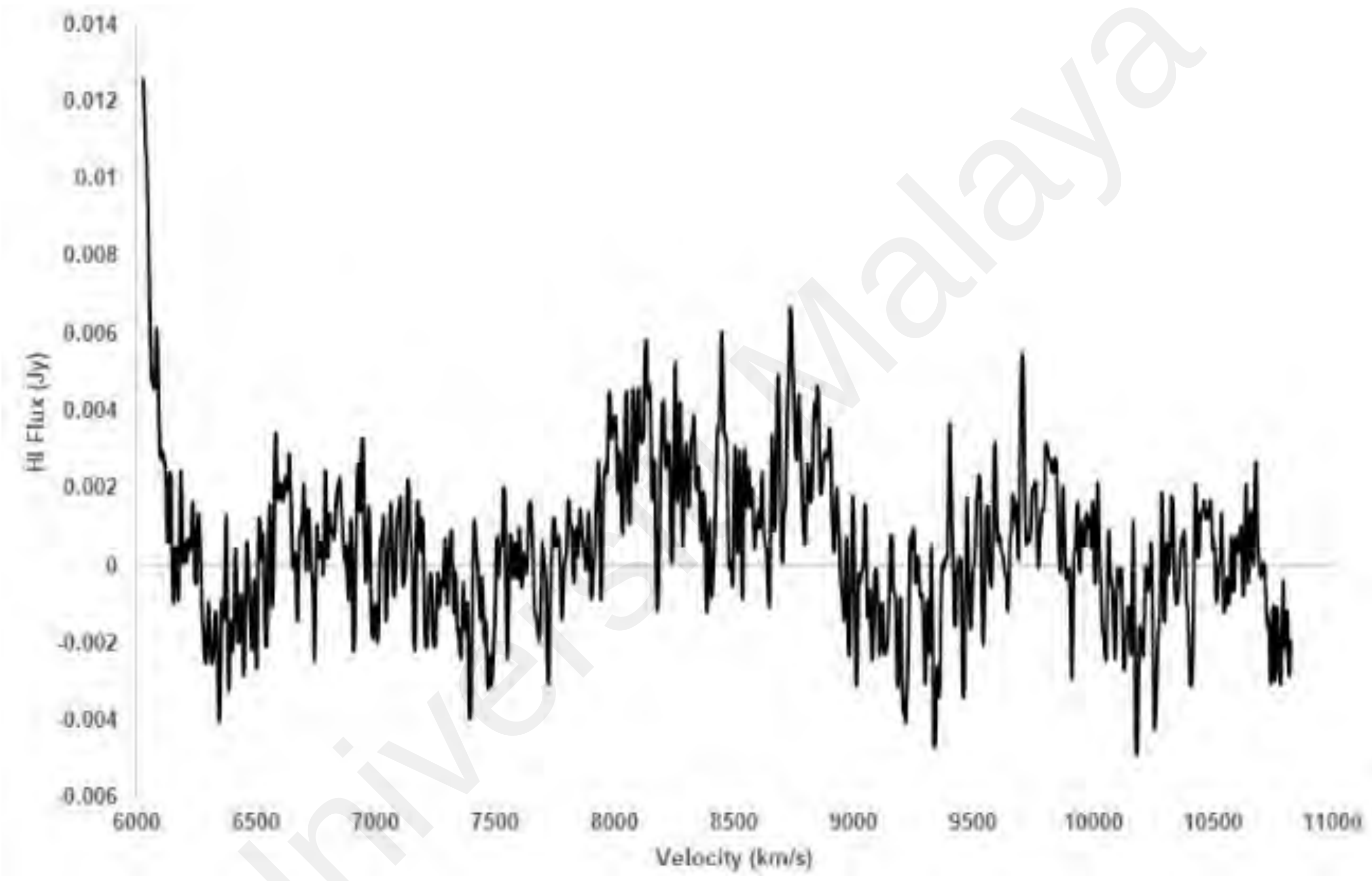

(b)

Figure 5.11: As in Figure 5.9, but for galaxy 7991-6104. The HI flux error is 332.0 mJy kms^{-1}.

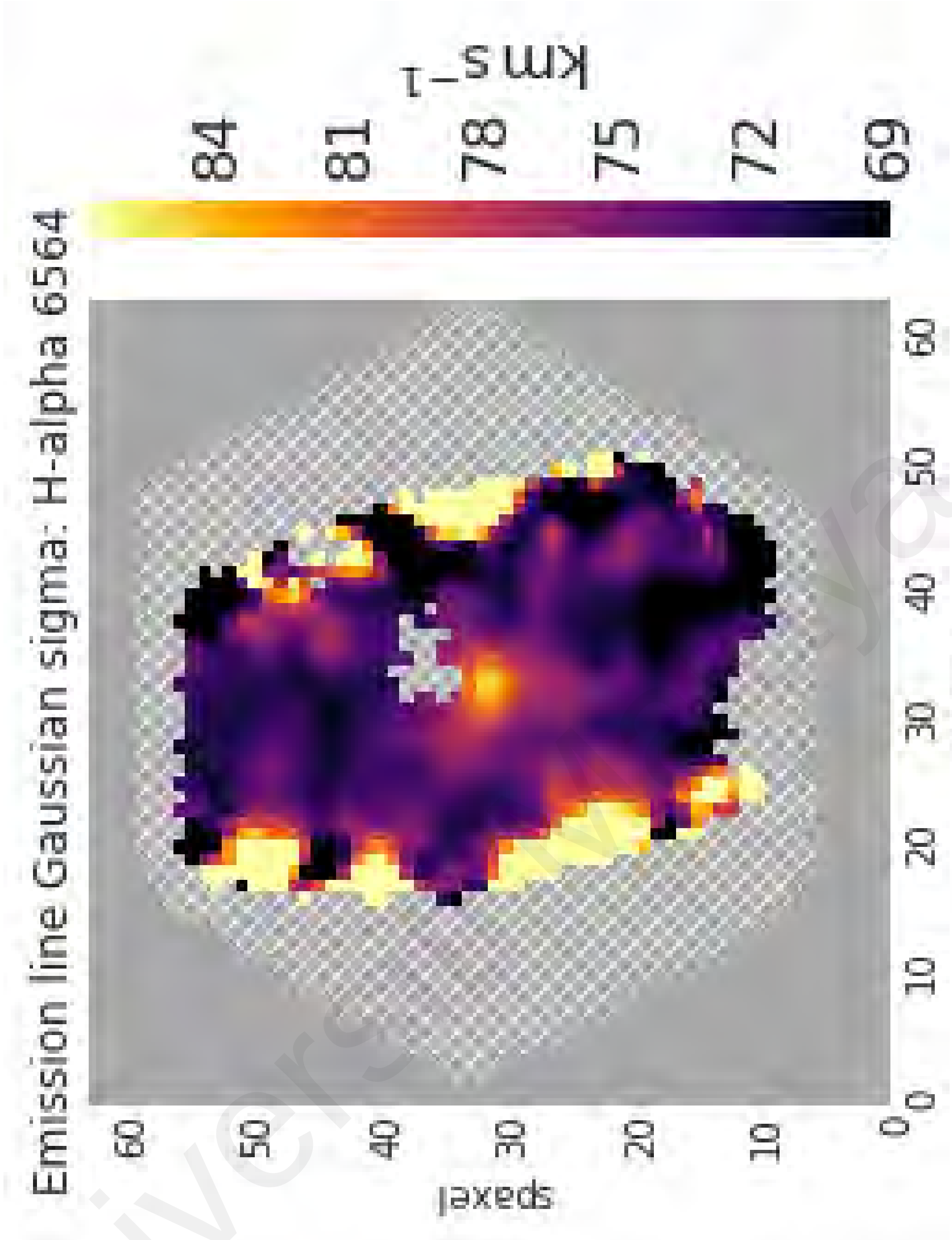
Emission line Gaussian sigma: H-alpha 6564
km s^{-1}
84
81
78
75
72
69
spaxel
spaxel
0
10
20
30
40
50
60

(a)

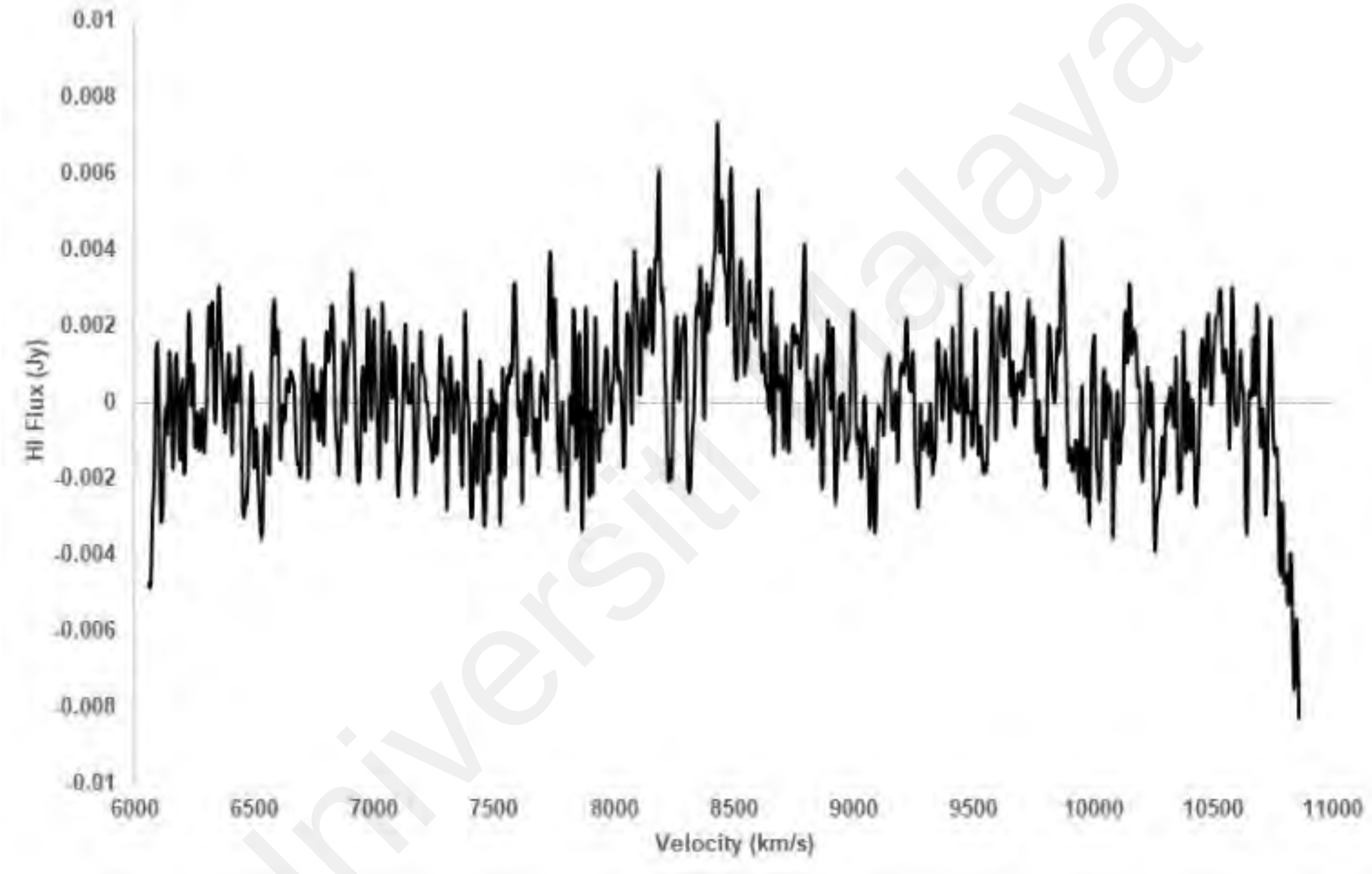

(b)

Figure 5.12: As in Figure 5.9, but for galaxy 7991-9101. The HI flux error is 332.0 mJy kms^{-1}.

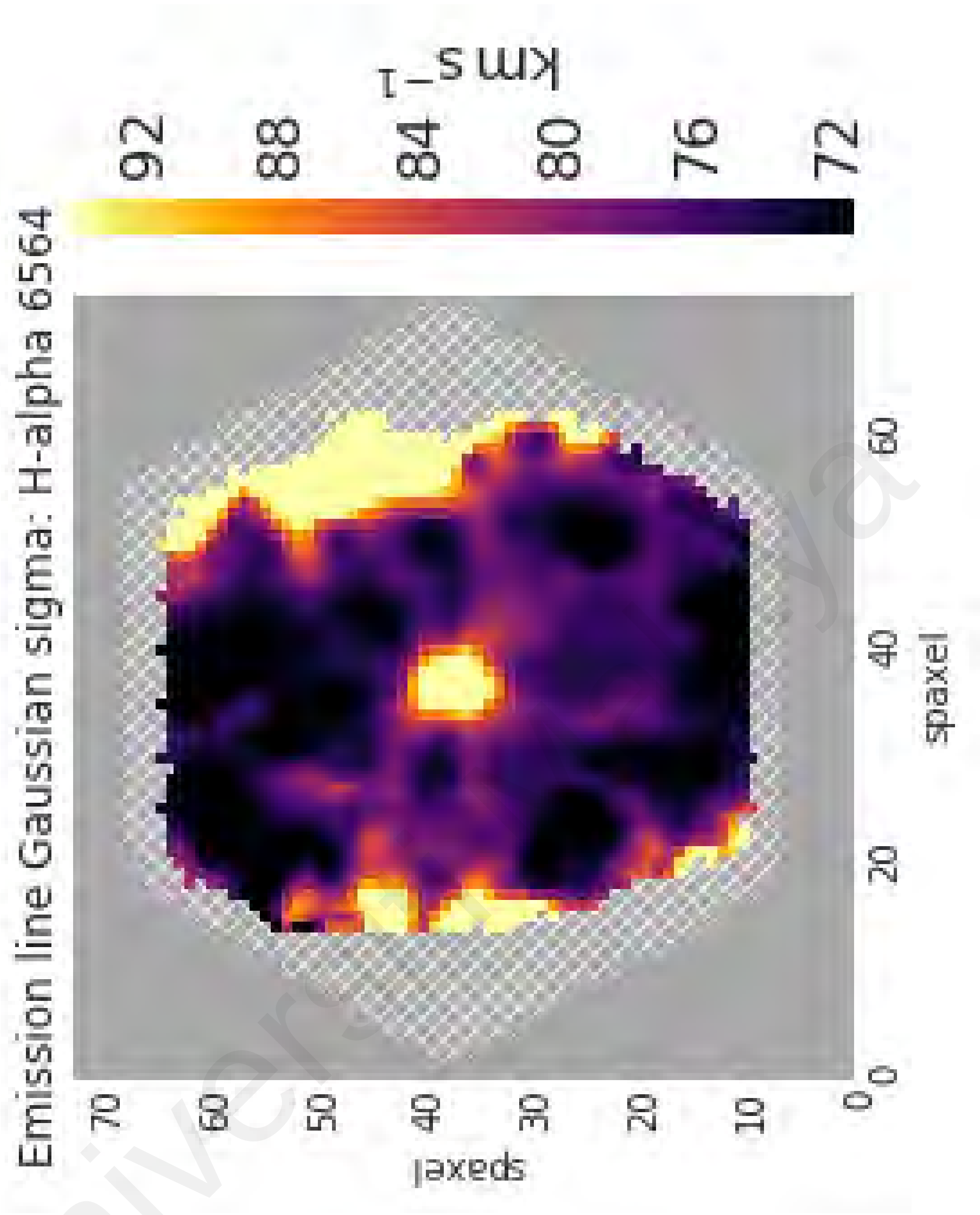
Emission line Gaussian sigma: H-alpha 6564
km s^{-1}
92
88
84
80
76
72
spaxel
70
60
50
40
30
20
10
0
spaxel
0
20
40
60

(a)

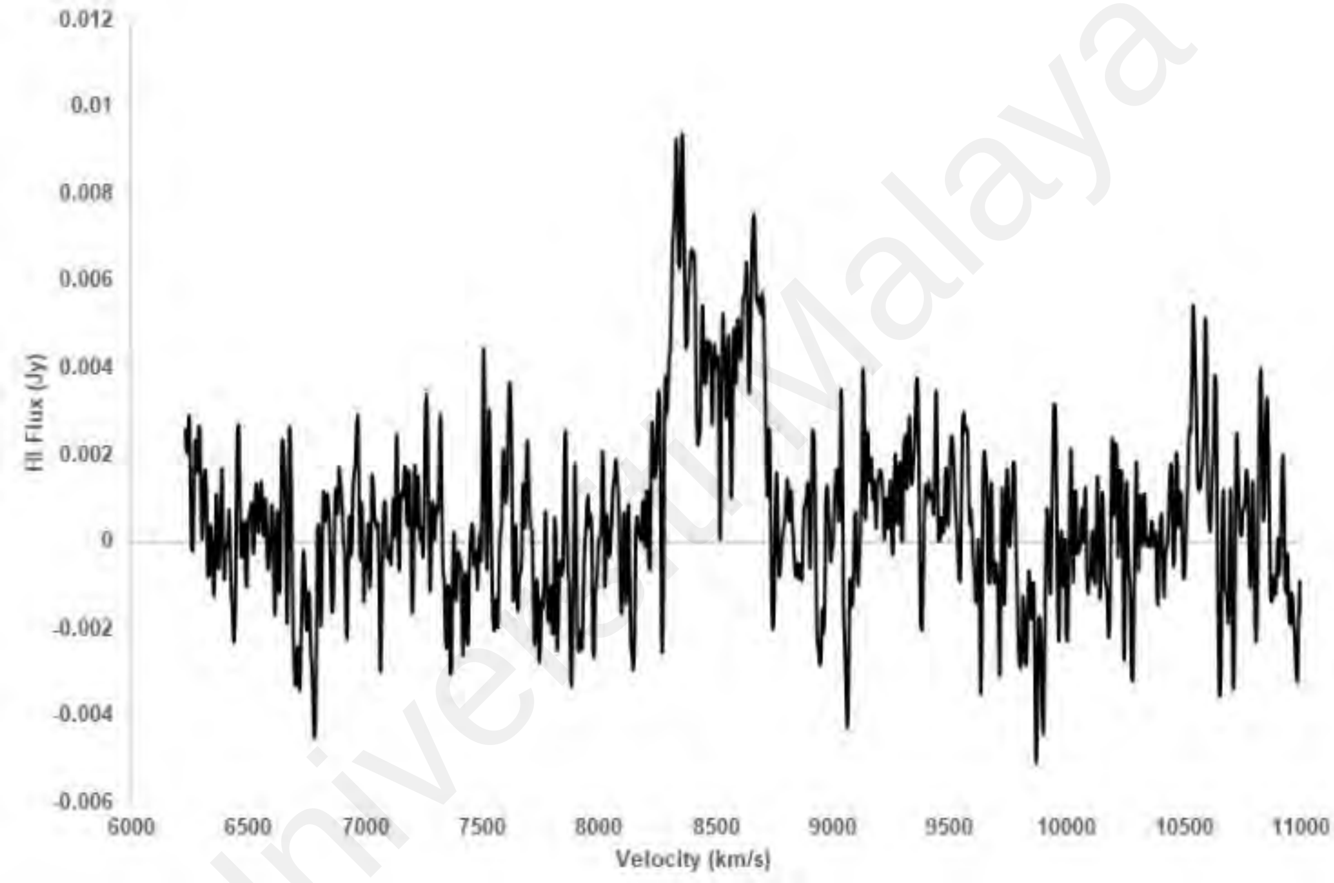

(b)

Figure 5.13: As in Figure 5.9, but for galaxy 7991-12701. The HI flux error is 332.0 mJy kms^{-1}.

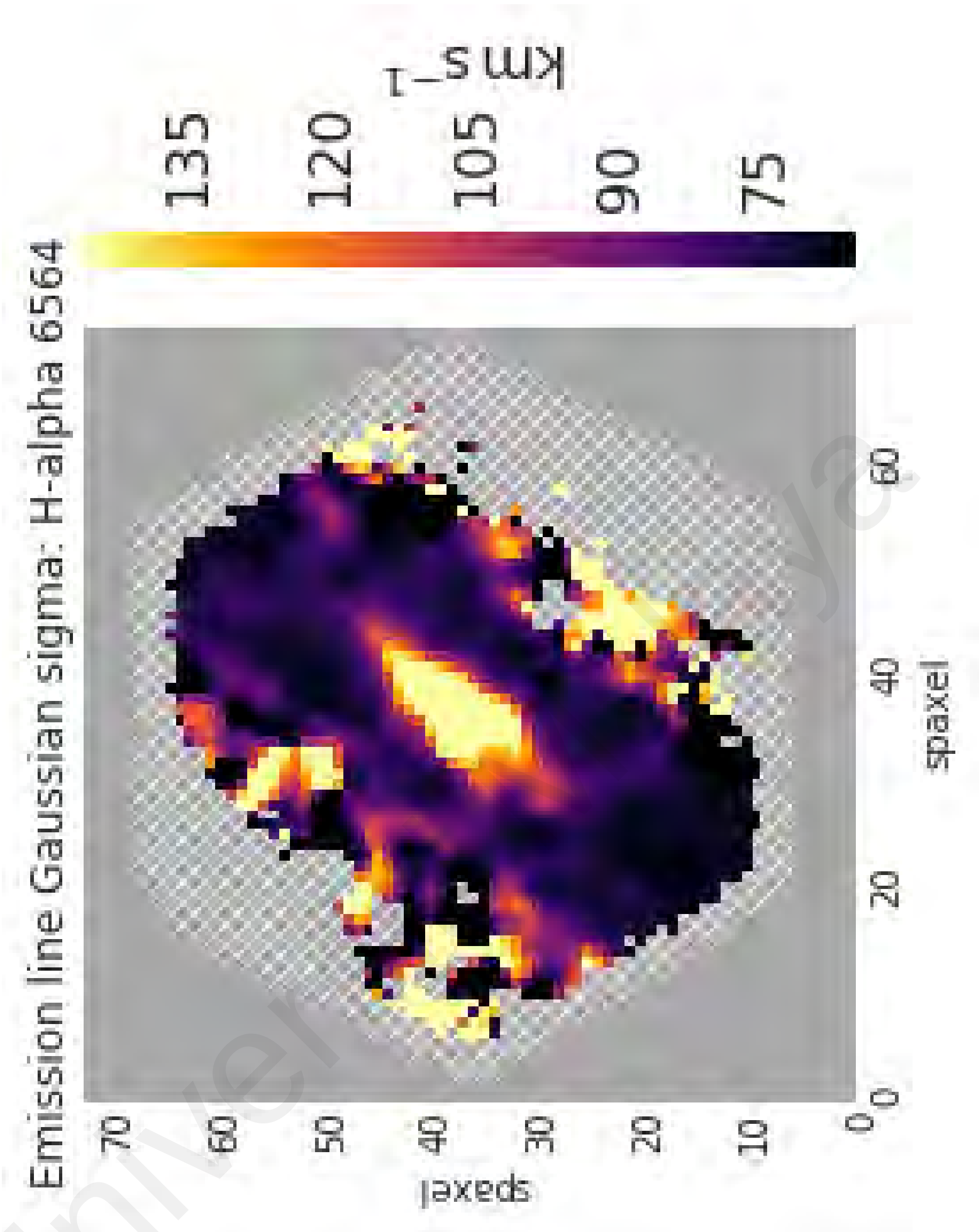

Emission line Gaussian sigma: H-alpha 6564
135
120
105
90
75
km s^{-1}
spaxel
spaxel

(a)

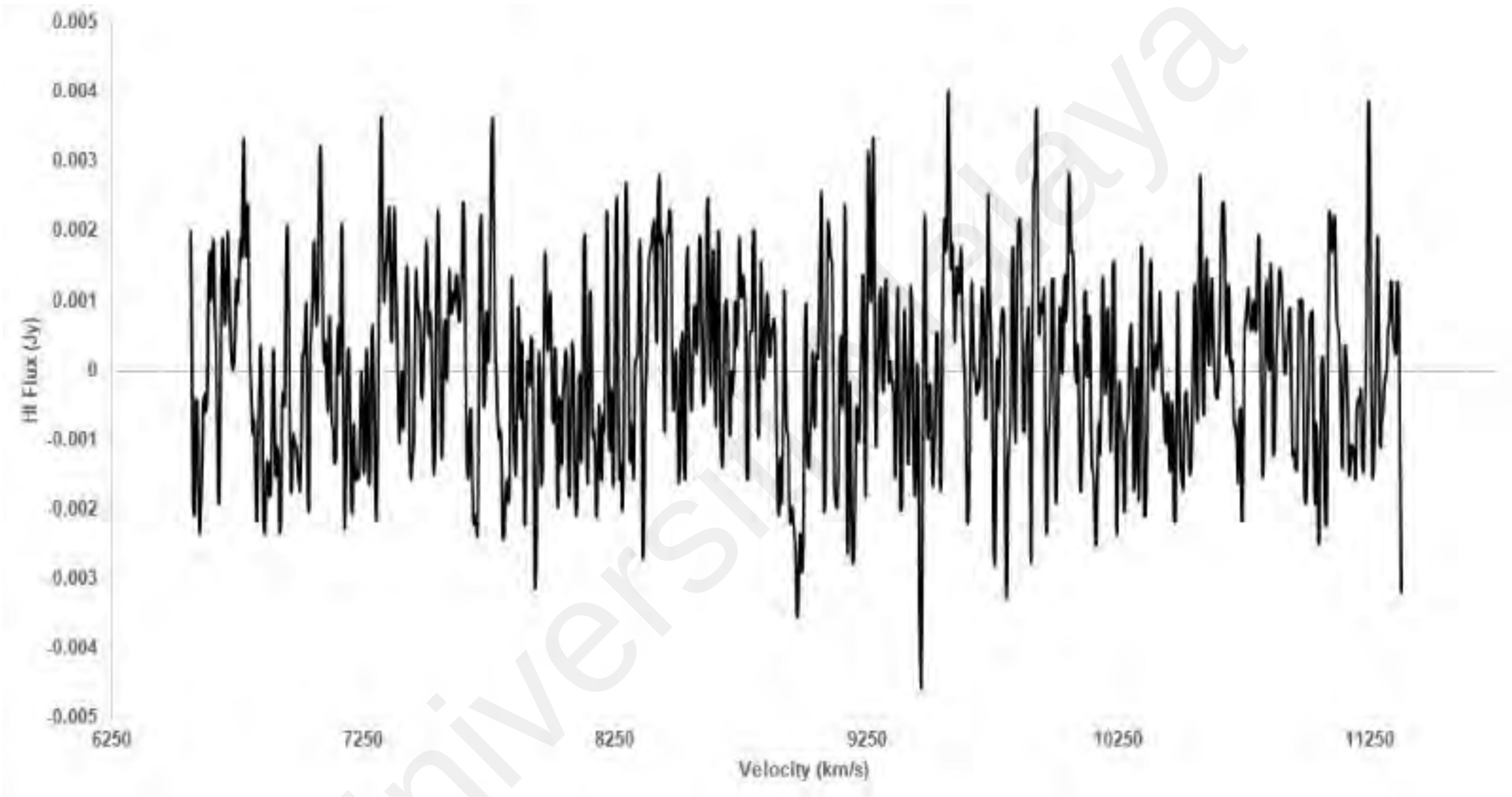

(b)

Figure 5.14: As in Figure 5.9, but for galaxy 7991-12703. The HI flux error is 332.0 mJy kms^{-1}.

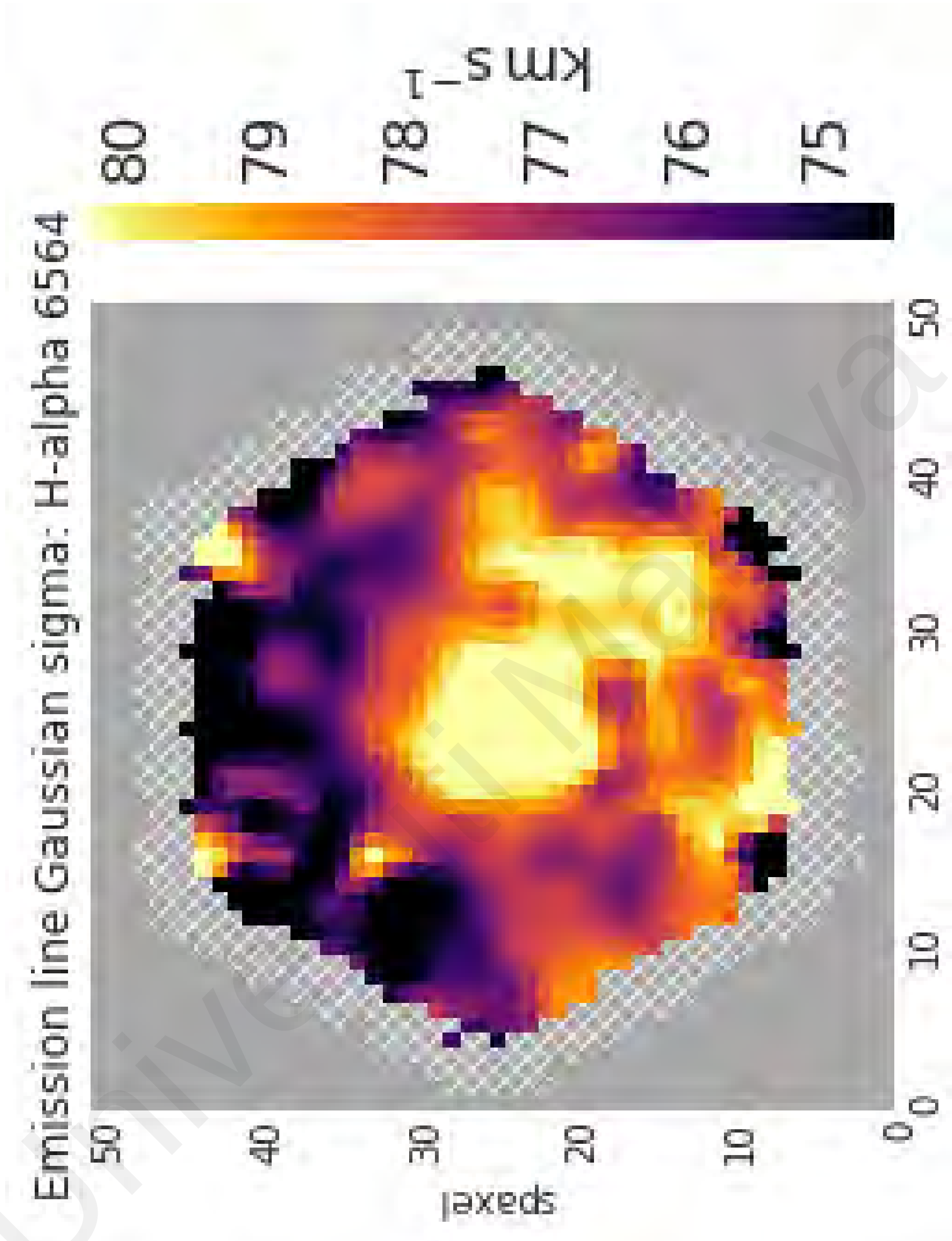

Emission line Gaussian sigma: H-alpha 6564
spaxel
spaxel
0
10
20
30
40
50
0
10
20
30
40
50
80
79
78
77
76
75
km s^{-1}

(a)

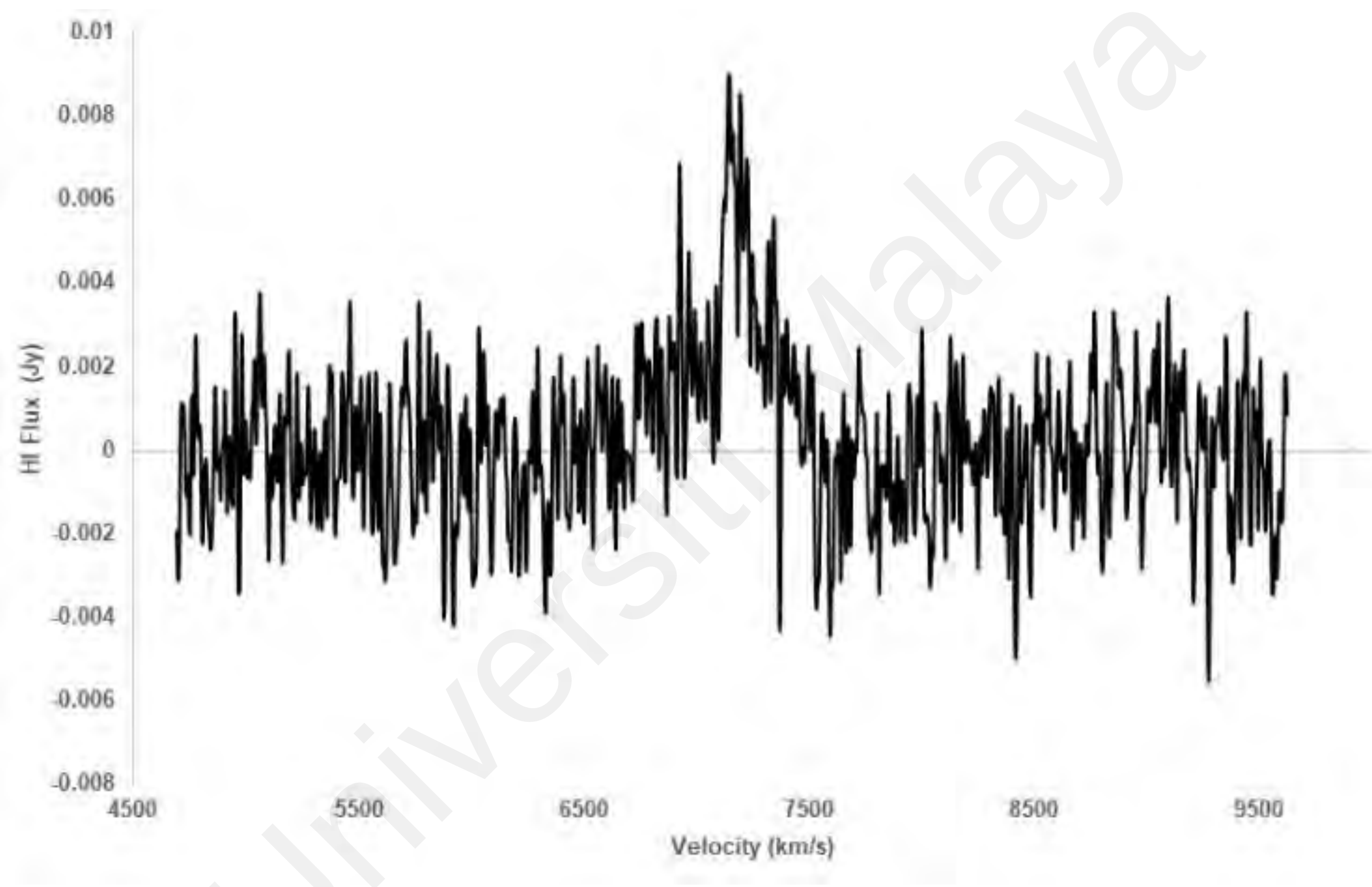

(b)

Figure 5.15: As in Figure 5.9, but for galaxy 8082-6103. The HI flux error is 332.0 mJy kms^{-1}.

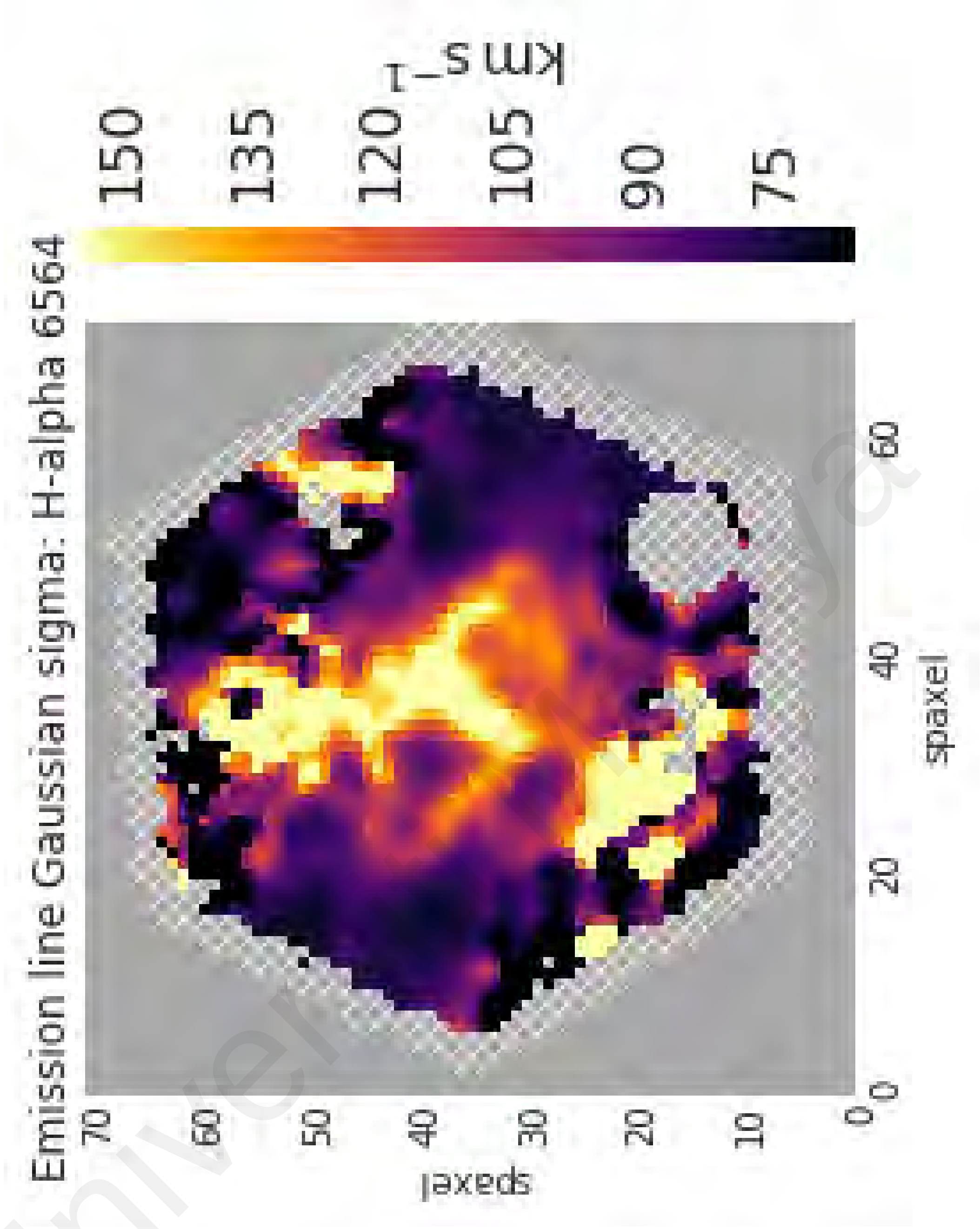

Emission line Gaussian sigma: H-alpha 6564
spaxel
spaxel
km s^{-1}
150
135
120
105
90
75
0
20
40
60
0
10
20
30
40
50
60
70

(a)

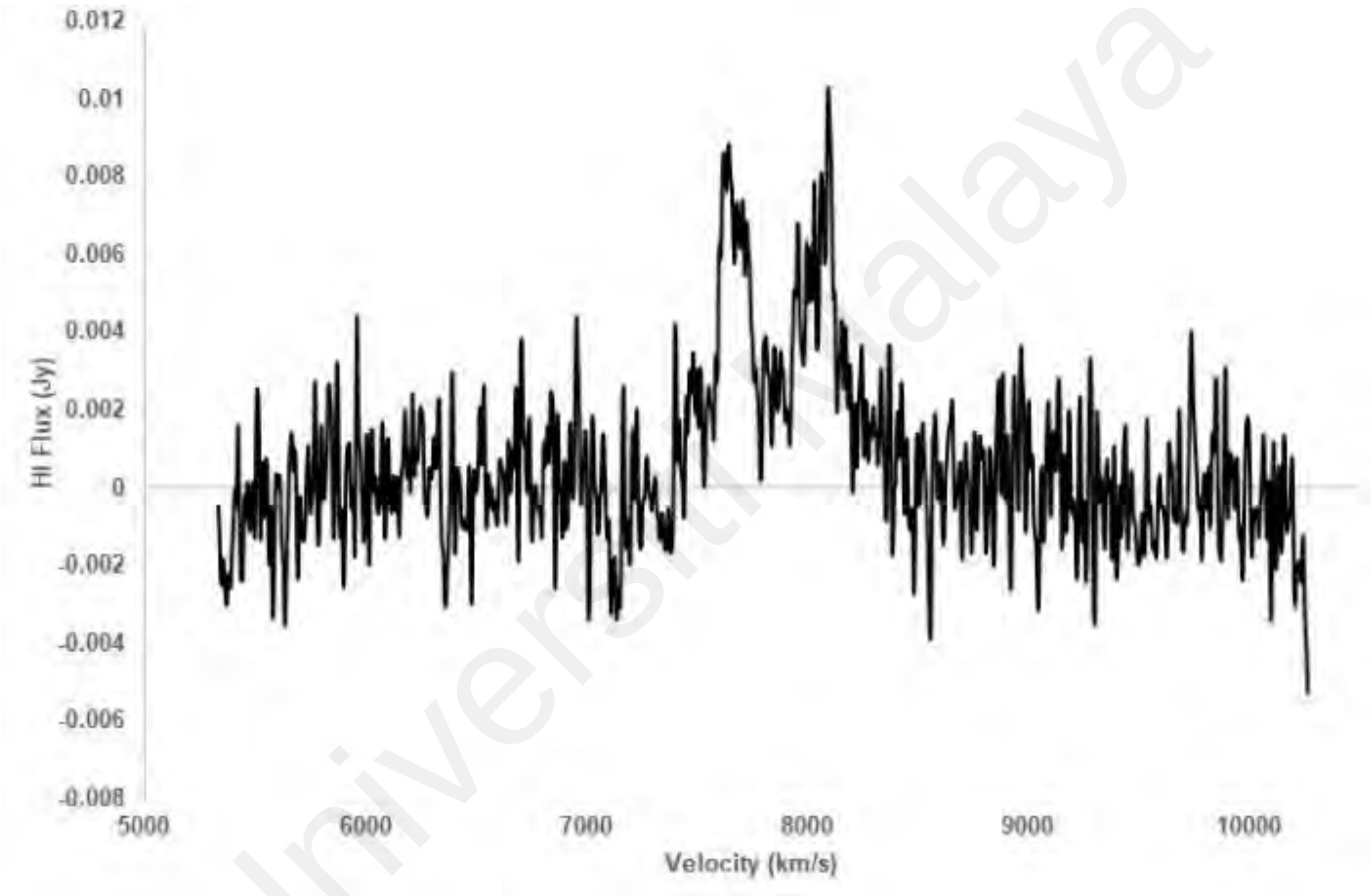

(b)

Figure 5.16: As in Figure 5.9, but for galaxy 8082-12702. The HI flux error is 332.0 mJy kms^{-1}.

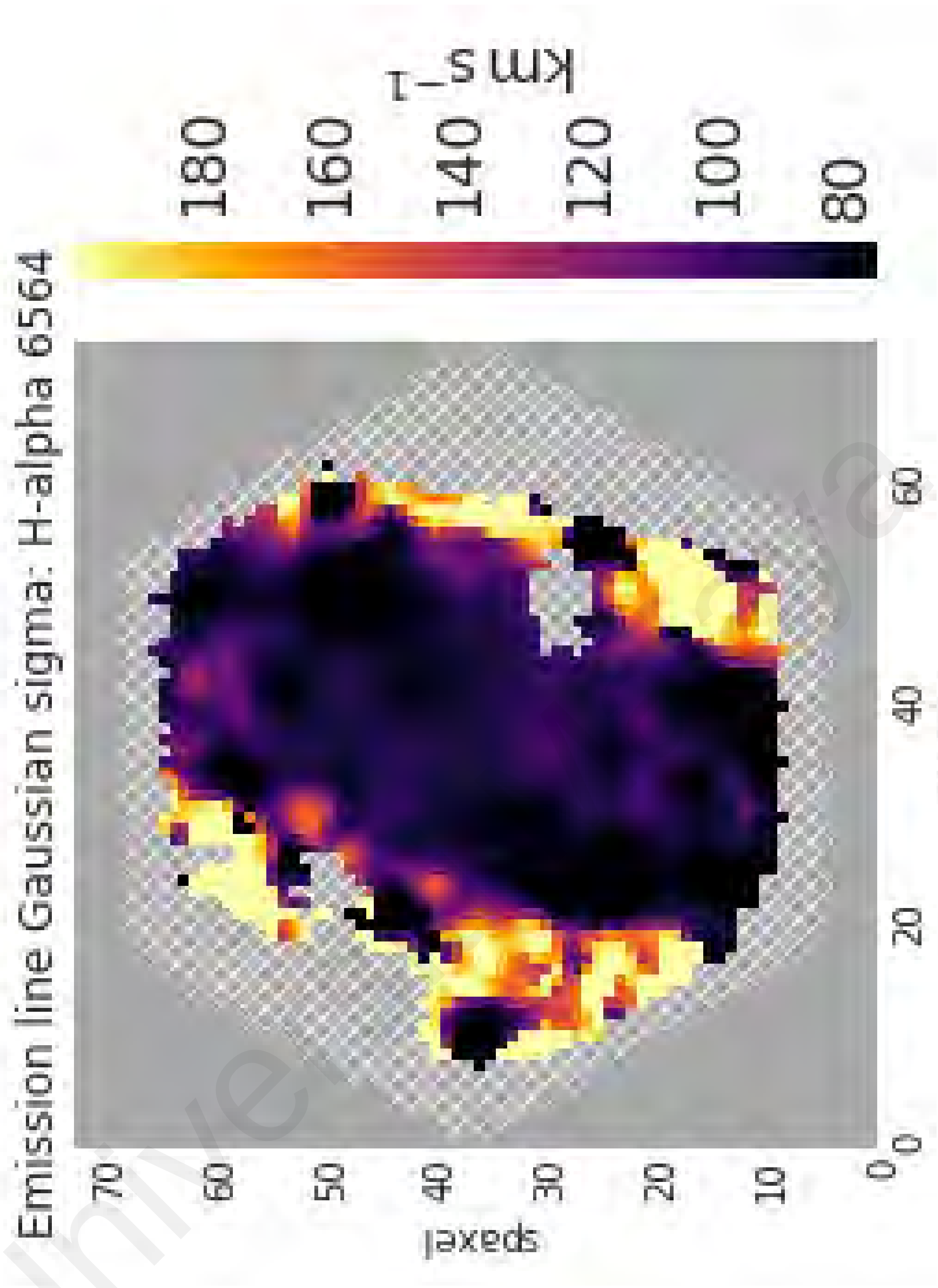
Emission line Gaussian sigma: H-alpha 6564
km s^{-1}
spaxel
spaxel

(a)

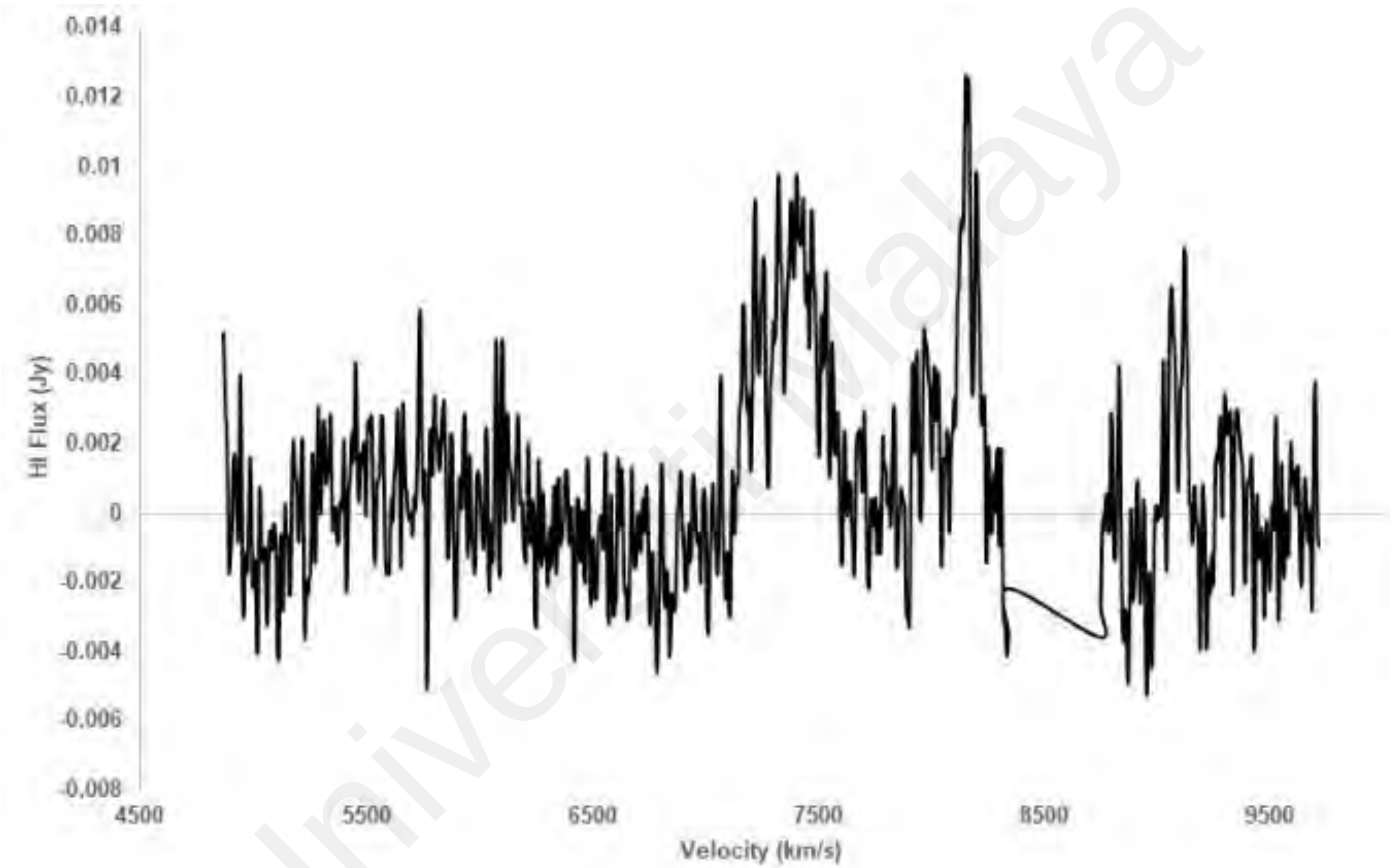

(b)

Figure 5.17: As in Figure 5.9, but for galaxy 8083-12703. The HI flux error is 332.0 mJy kms^{-1}.

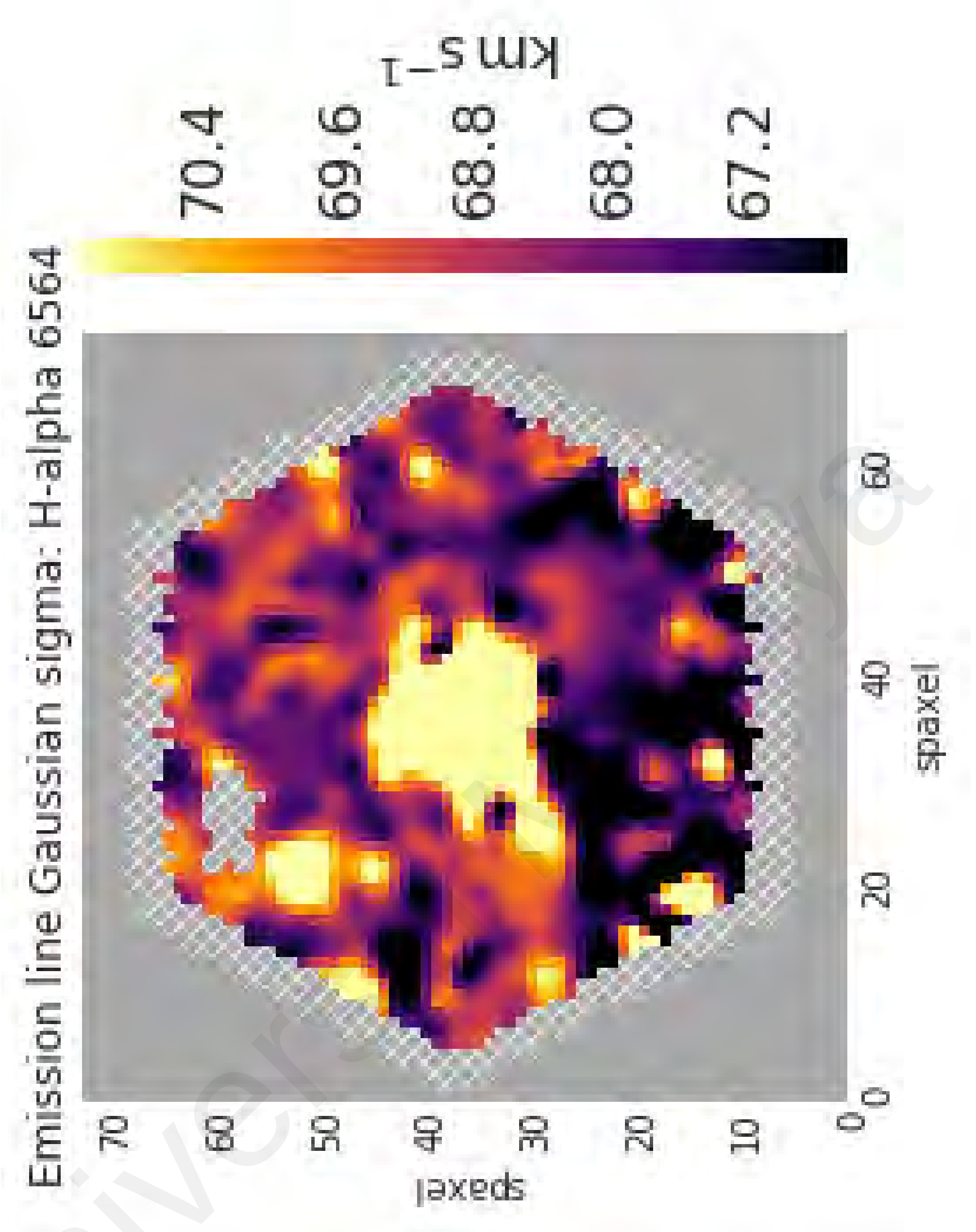
Emission line Gaussian sigma: H-alpha 6564
spaxel
spaxel
km s^{-1}
70.4
69.6
68.8
68.0
67.2

(a)

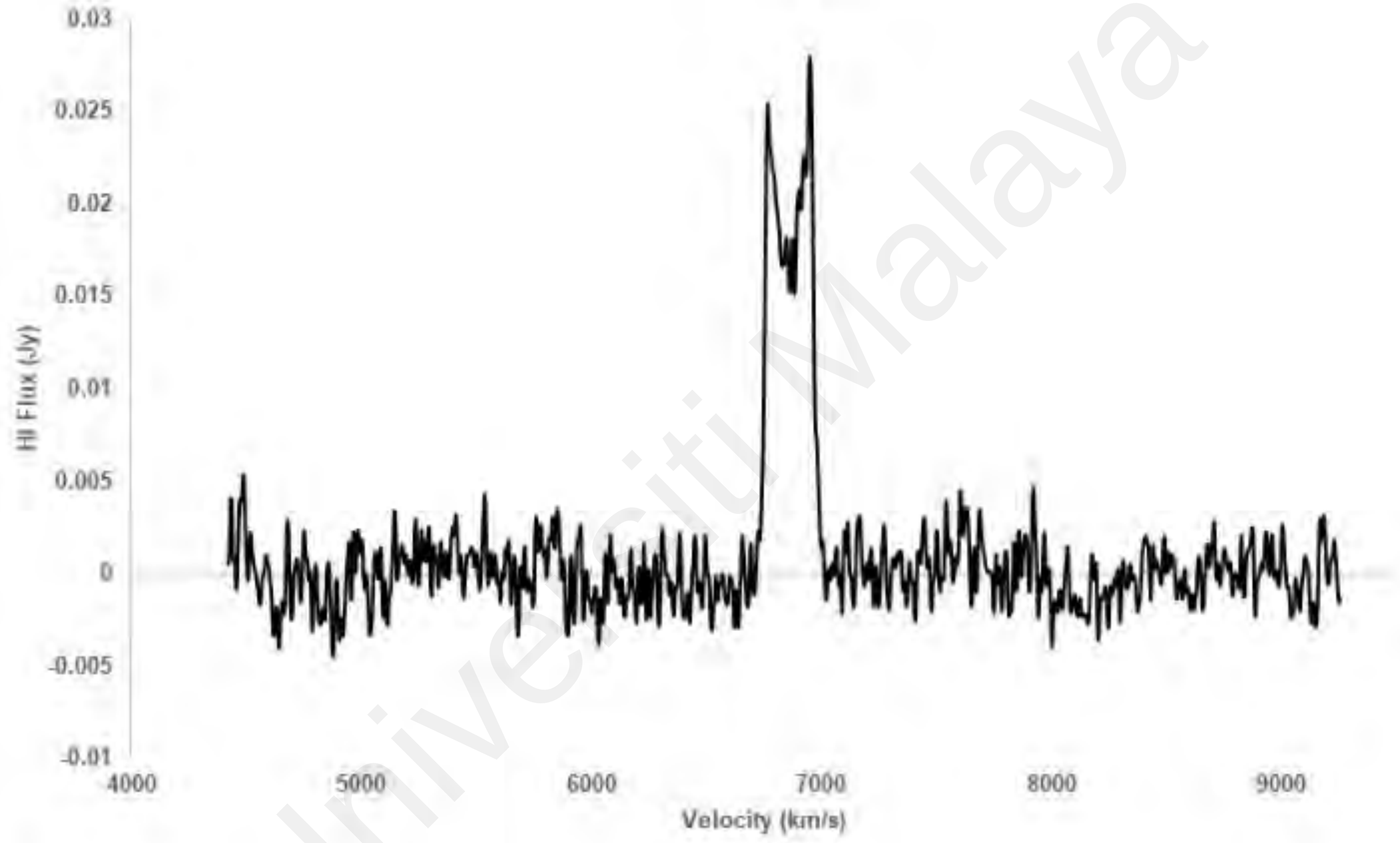

(b)

Figure 5.18: As in Figure 5.9, but for galaxy 8083-12704. The HI flux error is 332.0 mJy kms^{-1}.

The MaNGA sample of ten galaxies shows a correlation between the H-alpha velocities and the HI velocities. Galaxies that have a significant peak in their HI Spectra have a corresponding low H-alpha velocity and vice-versa. In galaxy 8083-12704, the HI Spectra has a peak emission of 0.03 Jy, with the H-alpha showing a peak velocity of 70.4 kms^{-1}. For galaxy 7991-3703, there is no HI Peak present in the spectra, but the H-alpha has a peak velocity of 350 kms^{-1}.

The case of galaxy 7991-3703 is particularly interesting as the MaNGA Integral Field Unit detectors indicates the high velocity of H-alpha. This is particularly interesting as H-alpha radiation is related to HI as the result of the de-excitation of the hydrogen atom and are often associated with star forming regions. In optical wavelengths, 7991-3703 has no obvious interacting partner and hence no tidal forces are suspected to be the cause of boosting the rotation speed of the H-alpha in the galaxy. The high h-alpha velocity, the rather spotty distribution of H-alpha emission and profile of the HI spectra might be indicative of rather vigorous star formation here. For the case of 7991-6104, it is a Seyfert galaxy (Véron-Cetty & Véron,2006), which could explain the H-alpha velocity of about 200 kms^{-1} in the central part of the galaxy. The presence of an AGN in this galaxy could also explain the shape of the HI spectra of this galaxy. Galaxy 7991-12703 seems to be rather deficient in HI based on its spectra. The central parts of the galaxy have the H-alpha moving at more than 135 kms^{-1}. In optical wavelengths, the galaxy is almost edge-on in its orientation towards Earth. This suggests that in this galaxy at least, much of the HI has been used up in star formation.

CHAPTER 6: DISCUSSION AND CONCLUSION

Radio observations of galaxy clusters searching for HI emission have concentrated on gas associated with individual cluster members through interferometry and have not been sensitive to any gas on scales larger than 1-3 arcmins. The small single dish observations are sensitive to larger spatial scales so should result in the detection of all of the neutral hydrogen in the cluster core and not just the gas bound to individual galaxies within the beam of the telescope. This should give a more complete picture of the HI content in these systems. As deduced from the velocity distribution of the member galaxies, any HI gas within any galaxy would result in a broader line width than observed in the three clusters observed using this method to date. Ram pressure and tidal stripping of HI gas from galaxies of all masses will respond to the dynamics of the local intracluster gas. Recent results from *Hitomi* (Aharonian et al. 2016) suggest that the local turbulence in the Intracluster Medium (ICM) is relatively small compared to the velocity dispersion of the cluster members (150-200 vs 1000-1500 km s^{-1}). Therefore, if HI gas stripped from galaxies can be shielded sufficiently from the strong X-ray emission from the ICM to prevent it being ionised, then diffuse, low velocity dispersion population of clouds could be present on 50 to 500 kpc scales. Another possible origin for HI in the cores of clusters is from the presence of a cooling flow. Evidence for cooling follows in clusters such as Perseus, as found by Sarazin (1988), includes the detection of a strong peak in the soft X-ray surface brightness at the cluster center and the measurement of inverted temperature gradient from extensive Chandra (Fabian et al. 2011) and XMM-Newton (Churazov et al. 2003) observations.

The cooling rate for Perseus was calculated to be about 30 to 50 Solar masses per year according to Peterson & Fabian (2006) and is significant in both A1367 and A262

(9.4 and 2.3 solar masses per year, White et al. (1997)). This offers the possibility of being a significant source of HI in the central 100 kpc of the cluster core. As cold molecular gas with a comparable velocity centroid and width has been detected from CO emission is the three clusters with single dish HI detections (Edge, 2001; Salome & Combes, 2003; Salome et al. 2008), it is possible that the detected HI and CO emitting gas arise from the same distribution of cold gas clouds.

Due to the fact that we obtain a comparable HI line detection in A262 (Hassan et al. 2016), A426 and a tentative detection in A1367, we can conclude that there may be a significant mass of atomic Hydrogen present in cluster cores that shares the dynamics of the intracluster medium and not the individual cluster members. Current interferometric searches and past observations with large single dishes would be insensitive to this gas so future smaller diameter single dish observations, may be the most efficient method to better characterise this gas in a larger sample with a diversity of gas cooling rates in their cores.

The use of a small single dish has revealed the presence of a significant mass of atomic hydrogen gas with a relatively narrow velocity dispersion in core of two nearby clusters of galaxies, A426 and A1367. The detected HI gas is not consistent with the velocity range of the gas-rich spirals known within each cluster leaving open the possibility that this cool atomic gas traces the gas stripped from cluster members or cooling out of the intracluster medium in the cores of the cluster. The HI gas mass obtained here is vitally important. Being the most abundant of the Baryonic matter, the HI mass is key towards applying the Virial theorem in order to move towards the deeper understanding of Dark Matter. The study of galaxy clusters is the study of the environment in which these galaxies reside.

The lessons here will also be applied on the UPSI-UM Radio Telescope. The use of the UPSI-UM Radio telescope in the future would allow much longer integration times per observed source. This would help increase the quality of the data obtained by reducing the rms error.

With regards to the ALMA results, from the definition of Compton-thick AGN, it is clear that there is more mass present in the central regions of this type of AGN. The presence of more mass can be implied from the higher velocities of that particular region. Looking at the rotation curves obtained for NGC 1068 in comparison with NGC 1097, the higher velocity of the CO gas at radius 0 kpc, can be taken as a possible identifying feature of Compton-thick AGN. This is in addition to the gradient or how steeply the velocity changes as the radius increases. However, a larger sample size needs to be studied to confirm this.

For the MaNGA sample, the trend seems to be the that the galaxies with the high velocity H-alpha tends to have little HI in them. This will become particularly useful and important in studying the gas dynamics on galactic scales. As explained earlier in this section, the importance of HI in Astrophysics cannot be overstated. The study of ALMA and MaNGA sample shows that in order to understand galaxy cluster dynamics, it is essential to study the gas dynamics of individual galaxies.

The conclusions of this thesis are:

1. The mass of HI in the Perseus cluster was calculated to be $(3.2 \pm 0.4) \times 10^{10}$ solar masses, with the Leo cluster having $(1.6 \pm 0.4) \times 10^{11}$ solar masses.
2. There is evidence that the velocity magnitude and gradient in the rotation curve can be utilised to help identify Compton-thick AGNs in the future.
3. The gas dynamics of H-alpha in the MaNGA sample is directly linked with the amount of HI gas in the galaxies.

REFERENCES

Aharonian, F., Akamatsu, H., Akimoto, F., Allen, S. W., Anabuki, N., Angelini, L., ... & Bamba, A. (2016). The quiescent intracluster medium in the core of the Perseus cluster. *Nature*, *535*(7610), 117-121.

Abell, G. O. (1958). The distribution of rich clusters of galaxies. *The Astrophysical Journal Supplement Series*, *3*, 211-290.

Abell, G. O., Corwin Jr, H. G., & Olowin, R. P. (1989). A catalog of rich clusters of galaxies. *The Astrophysical Journal Supplement Series*, *70*, 1-138.

Battye, R. A., Davies, R. D., & Weller, J. (2004). Neutral hydrogen surveys for high-redshift galaxy clusters and protoclusters. *Monthly Notices of the Royal Astronomical Society*, 355(4), 1339-1347.

Brinks, E., Skillman, E. D., Terlevich, R. J., & Terlevich, E. (1997). HI observations of NGC 1068. *Astrophysics and Space Science*, *248*(1-2), 23-31.

Brunzendorf, J., & Meusinger, H. (1999). The galaxy cluster Abell 426 (Perseus). A catalogue of 660 galaxy positions, isophotal magnitudes and morphological types. *Astronomy and Astrophysics Supplement Series*, *139*(1), 141-161.

Churazov, E., Forman, W., Jones, C., & Böhringer, H. (2003). XMM-Newton observations of the Perseus cluster. I. The temperature and surface brightness structure. *The Astrophysical Journal*, *590*(1), 225-237.

Conselice, C. J., Gallagher III, J. S., & Wyse, R. F. (2003). Galaxy Populations and Evolution in Clusters. III. The Origin of Low-Mass Galaxies in Clusters: Constraints from Stellar Populations. *The Astronomical Journal*, *125*(1), 66-85.

Cortese, L., Gavazzi, G., Boselli, A., Iglesias-Paramo, J., & Carrasco, L. (2004). Multiple merging in the Abell cluster 1367. *Astronomy & Astrophysics*, *425*(2), 429-441.

Davies, R. D., & Lewis, B. M. (1973). Neutral hydrogen in Virgo cluster galaxies. *Monthly Notices of the Royal Astronomical Society*, *165*(2), 231-244.

De Rijcke, S., Penny, S. J., Conselice, C. J., Valcke, S., & Held, E. V. (2009). Hubble Space Telescope survey of the Perseus cluster–II. Photometric scaling relations in different environments. *Monthly Notices of the Royal Astronomical Society*, *393*(3), 798-807.

Donnelly, R. H., Markevitch, M., Forman, W., Jones, C., David, L. P., Churazov, E., & Gilfanov, M. (1998). Temperature structure in abell 1367. *The Astrophysical Journal*, *500*(1), 138-146.

Dutson, K. L., Edge, A. C., Hinton, J. A., Hogan, M. T., Gurwell, M. A., & Alston, W. N. (2014). A non-thermal study of the brightest cluster galaxy NGC 1275–the Gamma-Radio connection over four decades. *Monthly Notices of the Royal Astronomical Society*, *442*(3), 2048-2057.

Ebeling, H., Stephenson, L. N., & Edge, A. C. (2014). Jellyfish: evidence of extreme ram-pressure stripping in massive galaxy clusters. *The Astrophysical Journal Letters*, *781*(2), L40-L45.

Edge, A. C. (2001). The detection of molecular gas in the central galaxies of cooling flow clusters. *Monthly Notices of the Royal Astronomical Society*, *328*(3), 762-782.

Edge, A. C., Stewart, G. C., Fabian, A. C., & Arnaud, K. A. (1990). An X-Ray Flux-Limited Sample of Clusters of Galaxies-Evidence for Evolution of the Luminosity Function. *Monthly Notices of the Royal Astronomical Society*, *245*, 559-569.

Fabian, A. C. (1994). Cooling flows in clusters of galaxies. *Annual Review of Astronomy and Astrophysics*, *32*(1), 277-318.

Fabian, A. C., Sanders, J. S., Ettori, S., Taylor, G. B., Allen, S. W., Crawford, C. S., ... & Ogle, P. M. (2000). Chandra imaging of the complex X-ray core of the Perseus cluster. *Monthly Notices of the Royal Astronomical Society*, *318*(4), L65-L68.

Fabian, A. C., Sanders, J. S., Allen, S. W., Canning, R. E. A., Churazov, E., Crawford, C. S., ... & Russell, H. R. (2011). A wide Chandra view of the core of the Perseus cluster. *Monthly Notices of the Royal Astronomical Society*, *418*(4), 2154-2164.

Fabian, A. C., Walker, S. A., Russell, H. R., Pinto, C., Sanders, J. S., & Reynolds, C. S. (2017). Do sound waves transport the AGN energy in the Perseus cluster?. *Monthly Notices of the Royal Astronomical Society: Letters*, *464*(1), L1-L5.

Fossati, M., Fumagalli, M., Boselli, A., Gavazzi, G., Sun, M., & Wilman, D. J. (2015). MUSE sneaks a peek at extreme ram-pressure stripping events–II. The physical properties of the gas tail of ESO137− 001. *Monthly Notices of the Royal Astronomical Society*, *455*(2), 2028-2041.

Gallimore, J. F., Baum, S., O'Dea, C., Brinks, E., & Pedlar, A. (2003). Neutral hydrogen absorption in NGC 1068 and NGC 3079. *Mass-Transfer Induced Activity in Galaxies*, 113-113.

Ge, C., Sun, M., Liu, R. Y., Rudnick, L., Sarazin, C., Forman, W., ... & Boselli, A. (2019). A merger shock in Abell 1367. *Monthly Notices of the Royal Astronomical Society: Letters*, *486*(1), L36-L40.

Gunn, J. E., & Gott III, J. R. (1972). On the infall of matter into clusters of galaxies and some effects on their evolution. *The Astrophysical Journal*, *176*, 1-17.

Hassan, M. S. R., Abidin, Z. Z., Ibrahim, U. F. S. U., Hashim, N., & Lee, D. A. A. (2016). Redshifts distribution in A262. *Monthly Notices of the Royal Astronomical Society*, *458*(1), 264-269.

Higdon, J. L., & Wallin, J. F. (2003). A minor-merger interpretation for NGC 1097's "Jets". *The Astrophysical Journal*, *585*(1), 281-297.

Impellizzeri, C. V., Gallimore, J. F., Baum, S. A., Elitzur, M., Davies, R., Lutz, D., ... & Sani, E. (2019). Counter-rotation and High-velocity Outflow in the Parsec-scale

Molecular Torus of NGC 1068. *The Astrophysical Journal Letters*, *884*(2), L28-L33.

Izumi, T., Kohno, K., Martín, S., Espada, D., Harada, N., Matsushita, S., ... & Imanishi, M. (2013). Submillimeter ALMA Observations of the Dense Gas in the Low-Luminosity Type-1 Active Nucleus of NGC1097. *Publications of the Astronomical Society of Japan*, *65*(5), 100-128.

Jin, Y., Zhu, L., Long, R. J., Mao, S., Wang, L., & van de Ven, G. (2019). SDSS-IV MaNGA: Internal mass distributions and orbital structures of early-type galaxies and their dependence on environment. *Monthly Notices of the Royal Astronomical Society*, *491*(2), 1690-1708.

Kalinova, V., Colombo, D., Rosolowsky, E., Kannan, R., Galbany, L., García-Benito, R., ... & Catalán-Torrecilla, C. (2017). Towards a new classification of galaxies: principal component analysis of CALIFA circular velocity curves. *Monthly Notices of the Royal Astronomical Society*, *469*(3), 2539-2594.

Lah, P., Pracy, M. B., Chengalur, J. N., Briggs, F. H., Colless, M., De Propris, R., ... & Tucker, B. E. (2009). The H i gas content of galaxies around Abell 370, a galaxy cluster at z= 0.37. *Monthly Notices of the Royal Astronomical Society*, *399*(3), 1447-1470.

Lim, J., Leon, S., & Combes, F. (2000). Molecular gas in the powerful radio galaxies 3c 31 and 3c 264: major or minor mergers? *The Astrophysical Journal Letters*, *545*(2), L93-L97.

Lin, L., Belfiore, F., Pan, H-A., Bothwell, M. S., Hsieh, P-Y., Huang, S., Xiao, T., Sánchez, S. F., Hsieh, B-C., Masters, K., Ramya, S., Lin, J-H., Hsu, C-H., Li, C., Maiolino, R., Bundy, K., Bizyaev, D., Drory, N., Ibarra-Medel, H., ... Thomas, D. (2017). SDSS-IV MaNGA-resolved star formation and molecular gas properties of green valley galaxies: a first look with ALMA and MaNGA. *The Astrophysical Journal*, *851*(1), 18-27.

Marinucci, A., Bianchi, S., Matt, G., Alexander, D. M., Baloković, M., Bauer, F. E., ... & Iwasawa, K. (2015). NuSTAR catches the unveiling nucleus of NGC 1068. *Monthly Notices of the Royal Astronomical Society: Letters*, *456*(1), L94-L98.

Masters, K. L., Stark, D. V., Pace, Z. J., Phipps, F., Rujopakarn, W., Samanso, N., ... & Cherinka, B. (2019). HI-MaNGA: HI Followup for the MaNGA Survey. *Monthly Notices of the Royal Astronomical Society, 488*(3)*,* 3396–3405.

Ondrechen, M. P., Van Der Hulst, J. M., & Hummel, E. (1989). HI in barred spiral galaxies. II-NGC 1097. *The Astrophysical Journal*, *342*, 39-48.

Onishi, K., Iguchi, S., Sheth, K., & Kohno, K. (2015). A Measurement of the Black Hole Mass in NGC 1097 Using ALMA. *The Astrophysical Journal*, *806*(1), 39-46.

Penny, S. J., Conselice, C. J., De Rijcke, S., & Held, E. V. (2009). Hubble Space Telescope survey of the Perseus Cluster–I. The structure and dark matter content of cluster dwarf spheroidals. *Monthly Notices of the Royal Astronomical Society*, *393*(3), 1054-1062.

Penny, S. J., Conselice, C. J., De Rijcke, S., Held, E. V., Gallagher III, J. S., & O'Connell, R. W. (2010). Hubble Space Telescope survey of the Perseus cluster–III. The effect of local environment on dwarf galaxies. *Monthly Notices of the Royal Astronomical Society*, *410*(2), 1076-1088.

Penny, S. J., Forbes, D. A., & Conselice, C. J. (2012). Hubble Space Telescope survey of the Perseus cluster–IV. Compact stellar systems in the Perseus cluster core and ultracompact dwarf formation in star-forming filaments. *Monthly Notices of the Royal Astronomical Society*, *422*(1), 885-901.

Peterson, J. R., & Fabian, A. C. (2006). X-ray spectroscopy of cooling clusters. *Physics Reports*, *427*(1), 1-39.

Prieto, M. A., Fernandez-Ontiveros, J. A., Bruzual, G., Burkert, A., Schartmann, M., & Charlot, S. (2019). From kpcs to the central parsec of NGC 1097: feeding star formation and a black hole at the same time. *Monthly Notices of the Royal Astronomical Society*, *485*(3), 3264-3276.

Roberts, M. S. (1962). The neutral hydrogen content of late-type spiral galaxies. *The Astronomical Journal*, *67*, 437-446.

Salome, P., & Combes, F. (2003). Cold molecular gas in cooling flow clusters of galaxies. *Astronomy & Astrophysics*, *412*(3), 657-667.

Salomé, P., Combes, F., Revaz, Y., Edge, A. C., Hatch, N. A., Fabian, A. C., & Johnstone, R. M. (2008). Cold gas in the Perseus cluster core: Excitation of molecular gas in filaments. *Astronomy & Astrophysics*, *484*(2), 317-325.

Sarazin, C. L. (1986). X-ray emission from clusters of galaxies. *Reviews of Modern Physics*, *58*(1), 1-153.

Schröder, A., Drinkwater, M. J., & Richter, O. G. (2001). The neutral hydrogen content of Fornax cluster galaxies. *Astronomy & Astrophysics*, *376*(1), 98-111.

Solanes, J. M., Manrique, A., García-Gómez, C., González-Casado, G., Giovanelli, R., & Haynes, M. P. (2001). The HI content of spirals. II. Gas deficiency in cluster galaxies. *The Astrophysical Journal*, *548*(1), 97-114.

Sun, M., & Murray, S. S. (2002). Chandra View of the Dynamically Young Cluster of Galaxies A1367. I. Small-Scale Structures. *The Astrophysical Journal*, *576*(2), 708-720.

Tabatabaei, F. S., Minguez, P., Prieto, M. A., & Fernández-Ontiveros, J. A. (2018). Discovery of massive star formation quenching by non-thermal effects in the centre of NGC 1097. *Nature Astronomy*, *2*(1), 83-89.

Tanaka, I., Yagi, M., & Taniguchi, Y. (2017). Morphological evidence for a past minor merger in the Seyfert galaxy NGC 1068. *Publications of the Astronomical Society of Japan*, *69*(6), 90-106.

Tsai, M., Hwang, C. Y., Matsushita, S., Baker, A. J., & Espada, D. (2012). Interferometric CO (3–2) observations toward the central region of NGC 1068. *The Astrophysical Journal*, *746*(2), 129-139.

Teodoro, E. D., & Fraternali, F. (2015). 3D BAROLO: a new 3D algorithm to derive rotation curves of galaxies. *Monthly Notices of the Royal Astronomical Society*, *451*(3), 3021-3033.

White, D. A., Jones, C., & Forman, W. (1997). An investigation of cooling flows and general cluster properties from an X-ray image deprojection analysis of 207 clusters of galaxies. *Monthly Notices of the Royal Astronomical Society*, *292*(2), 419-467.

Williams, D. R. W. (1973). Studies of four regions for use as standards in 21 CM observations. *Astronomy and Astrophysics Supplement Series*, *8*, 505-516.